REVISION 1

Trace-element partitioning between plagioclase, alkali feldspar, Ti-magnetite, biotite, apatite and evolved potassic liquids from Campi Flegrei (Southern Italy).

Lorenzo Fedele[1], Michele Lustrino[2,3], Leone Melluso[1], Vincenzo Morra[1], Alberto Zanetti[4] and Riccardo Vannucci[5]

[1]Dipartimento di Scienze della Terra, dell'Ambiente e delle Risorse, Università degli Studi di Napoli Federico II, Via Mezzocannone 8, 80134 Napoli, Italy

[2]Dipartimento di Scienze della Terra, Università degli Studi di Roma La Sapienza, Piazzale Aldo Moro 5, 00185 Roma, Italy

[3]CNR, Istituto di Geologia Ambientale e Geoingegneria (IGAG), c/o Dipartimento di Scienze della Terra, Università degli Studi di Roma La Sapienza, P.le A. Moro, 5, 00185 Roma, Italy

[4]CNR, Istituto di Geoscienze e Georisorse (IGG), U.O.S. di Pavia, Via Ferrata 1, 27100 Pavia, Italy

[5]Dipartimento di Scienze della Terra e dell'Ambiente, Università di Pavia, Via Ferrata 1, 27100 Pavia, Italy

Abstract

Partition coefficients ($^{Min/L}D$) for a series of geochemically relevant elements have been calculated from combined EMP/LA-ICP-HRMS analyses of plagioclase, alkali feldspar, Ti-magnetite, biotite, apatite and trachytic/trachyphonolitic melt pairs in selected Campi Flegrei pyroclastic rocks. $^{Pl/L}D$ and $^{Kfs/L}D$ values are generally very low for most of the trace-elements but Sr, Ba and Eu. The $^{Kfs/L}D$ for the latter elements record a systematic increase as the melt

composition changes from trachyte to trachyphonolite, likely due to increasing structural compliance of the sanidine in the trachyphonolites related to larger Na/K values. Conversely, $^{Kfs/L}D$ values for transitional, highly-charged incompatible elements (e.g., LREE) decrease from trachyte to trachyphonolite, possibly in response to the decrease of melt polymerization. $^{Min/L}D$ values for titanomagnetite generally decrease with the increasing melt evolution, the highest values being those measured for Ti, V and Sc. Titanium, Ba, Sc, Rb, Nb, Ta and V are compatible in biotite in equilibrium with trachytic melt, whereas Cs, Sr and Pb are incompatible and REE are strongly incompatible, as supported by the extremely low $^{Bt/L}D_Y$ (0.003-0.008). Partition coefficients for apatite and trachyphonolitic glass pairs are high for Sr, REE (particularly MREE) and Y, large for Th, U and V, generally low for HFSE and variable for other LILE. The comparison of measured $^{Min/L}D$ values for Campi Flegrei trachytes/trachyphonolites with other sets of partition coefficients reported in literature for evolved potassic systems suggests that a reliable dataset for magma evolution modelling requires: (i) a thorough preliminary selection of natural samples; (ii) the adoption of accurate microanalytical techniques; (iii) the direct measurement of $^{Min/L}D$ values for each specific melt composition.

Keywords: Campi Flegrei, partition coefficients, plagioclase, alkali feldspar, Ti-magnetite, biotite, apatite, LA-ICP-HRMS

Introduction

Although trace-element partition coefficients are a powerful and widely used tool in modelling the evolution of magmatic systems, reliable datasets that describe the trace-element partitioning behaviour in highly differentiated potassic alkaline liquids are still scarce or lacking. In a companion paper, Fedele et al. (2009) reported the results of detailed EMP/LA-ICP-HRMS investigations aimed at obtaining an internally consistent set of trace-element partition coefficients for clinopyroxene/melt

pairs from selected Campi Flegrei trachytic/trachyphonolitic samples. These samples resulted particularly suitable for partitioning studies in virtue of their glassy nature and their moderately porphyritic character. In addition, the employed microanalytical technique allowed the authors to reliably assess the attainment of mineral/glass chemical equilibrium and to consequently recognize suitable sites for the correct evaluation of the mineral/liquid partition coefficients. Major- and trace-element analyses of plagioclase, alkali feldspar, Ti-magnetite, biotite and apatite from the same Campi Flegrei samples investigated by Fedele et al. (2009) are here presented in order to complete the study on the trace-element partitioning for the typical paragenesis of evolved potassic melts.

Geological background

The Campi Flegrei is an active volcanic field covering an area running from the city of Naples to its western suburbs, whose last eruption occurred in AD 1538 (D'Oriano et al. 2005 and references therein). Fumarolic and hydrothermal phenomena (plus sporadic bradiseismic crises) are the only evidence of ongoing a volcanic activity, which has been predominantly explosive, characterized by a great number of eruptions building numerous (mainly monogenetic) volcanic edifices and very rare effusive manifestations of limited areal extent (e.g., Morra et al. 2010; Melluso et al. 2012 and references therein). The Campi Flegrei district is characterized by a nested caldera structure whose genesis is attributed to the two most explosive events of the area (Perrotta et al. 2006): the Ignimbrite Campana (IC, ~39 ka; De Vivo et al. 2001) and the Tufo Giallo Napoletano (TGN, ~15 ka; Deino et al. 2004) eruptions.

Campi Flegrei juvenile products have a potassic alkaline affinity, belonging to the slightly silica-undersaturated shoshonitic series of the "orogenic" Italian Plio-Pleistocene Roman Province (e.g., Lustrino et al. 2011 and references therein). Rock compositions range from rare

shoshonitic basalts to predominant trachytes-trachyphonolites-phonolites (e.g., Morra et al. 2010 and references therein).

The investigated samples belong to the Breccia Museo Formation (BM; Perrotta and Scarpati 1994; Melluso et al. 1995; Fedele et al. 2008), interpreted as the proximal facies deposit of the IC eruption (Fedele et al. 2008 and references therein). The juvenile products of the BM are pumices, obsidians and spatter clasts, showing trachytic to phonolitic compositions. The phenocryst load is generally ~5-12% (estimated as the area occupied by phenocrysts over a total area of a thin section), represented mainly by sanidine, plagioclase, clinopyroxene, biotite, opaque oxides and apatite (in decreasing order of abundance) set in a completely glassy groundmass (Fig. 1).

Analytical techniques

The major element composition of the mineral phases and the glassy matrix has been determined by Electron Microprobe analyses (EMP) at the CNR-IGAG (Rome, Italy), using an automated CAMECA SX50 microprobe in full WDS mode. An acceleration potential of 20 kV with a sample current of 20 nA (measured on brass) was applied. The beam size was varied as a function of the analyzed phase, with a particularly large beam size (300 μm^2) for the glass phases. Natural and synthetic oxides and silicates were used as standards. On-line corrections for drift, dead-time and background were applied to the raw data. Precision is 2% (relative).

Trace-element contents in mineral phases and host glass were determined on 100 μm-thick thin sections by Laser Ablation - Inductively Coupled Plasma – High Resolution Mass Spectrometry (LA-ICP-HRMS) at IGG-CNR (Pavia, Italy). The microprobe consists of a double-focusing sector-field analyzer (Finnigan Mat, Element I) coupled with a Q-switched Nd:YAG laser source (Quantel Brilliant). The fundamental emission of the laser source (1064 nm, in the

near-IR region) was converted to 213 nm by three harmonic generators. Helium was used as carrier gas and mixed with Ar downstream of the ablation cell. Spot diameter was varied in the range of 40-60 μm. Quantification was carried out using the NIST SRM 610 glass as external standard (Pearce et al. 1996). Si was used as internal standard for plagioclase, K-feldspar, biotite and glass, while Ca was used for apatite and Ti for magnetite. Detection limits are in the range 100-500 ppb for Sc, Ti and Cr, 10-100 ppb for V, Rb, Sr, Zr, Cs, Ba, Gd and Pb, 1-10 ppb for Y, Nb, La, Ce, Nd, Sm, Eu, Tb, Dy, Er, Yb, Hf and Ta, and usually <1 ppb for Pr, Ho, Tm, Lu, Th and U. Precision and accuracy (both better than 10% for concentrations at ppm level) were assessed by means of repeated analyses of NIST SRM 612 and BCR-2g standards. The composition of the glass beneath the thin section has been documented before the sample analysis in order to promptly recognize the piercing of the rock and to eliminate any glass contribution. The gas background was measured for 60 s, as in any other routine analysis, whereas signals during ablation were acquired for approximately 20-50 s. Analyses were performed with 10 Hz repetition rate of laser and ~1-2.5 mJ/sec laser power. Full details as in Miller et al. (2007).

Precautions have been taken to avoid any bias on the analytical results. Memory effects have been taken into account leaving more than one minute between two consecutive analyses and analyzing glasses after the minerals. Spurious signals related to memory effects usually affect more blanks (because less time is passed after the previous analysis), thus determining a worsening of the detection limits and hindering the quantification of elements at ultra-trace concentration level. Surface contamination during sample polishing and/or handling before the micro-analytical measurement and occurrence of micro-inclusions of glass/fluid have been monitored by detailed inspection of the signal profiles acquired during ablation. Only intervals with parallel signals have been integrated. Anomalous signal contributions at the beginning of the

ablation (due to surface contamination) and/or randomly occurring during ablation (possibly related to inclusions and/or memory effect) has been accurately documented and excluded by integration.

Results

The selected BM juvenile samples (Melluso et al. 1995) are single obsidian (samples AI, AN and I) and single spatter (B, C and R) clasts, about 15-20 cm in diameter (Fig. 1). Following the R_1R_2 classification diagram (De La Roche et al. 1980; Fig. 2), rocks are trachytes (AI, AN and C, plotting as trachytes in the TAS diagram) and trachyphonolites (B, I and R, phonolites in the TAS diagram). Trachytic samples are vitrophyric (phenocryst load ~10-12%), with phenocrysts of sanidine (~50-55%), clinopyroxene (~15-20%), plagioclase (~15-20%), biotite (~5-10%) and magnetite (<1%) set in a glassy matrix. Trachyphonolitic samples are also vitrophyric and have lower phenocryst load (≤5%) and a phenocrysts assemblage consisting of sanidine (~75%), plagioclase (~15-20%) and clinopyroxene (~5-8%) plus accessory magnetite, biotite and apatite. An increase of SiO_2 (from 58.9-59.8 to 60.4-60.7 wt%), Na_2O (2.61-3.36 to 6.25-6.45 wt%), incompatible elements (e.g., Zr from 175-255 to 681-733 ppm, La 38-48 to 116-119 ppm) and P.I. [0.77-0.81 to 0.95-0.97; P.I. = peralkaline index = molar (Na+K)/Al], associated with a decrease of MgO (from 1.08-1.73 to 0.37-0.92 wt%), CaO (2.53-3.14 to 1.62-1.78 wt%), K_2O (9.14-9.52 to 7.17-7.22 wt%), Ba (519-1210 to 23-93 ppm) and Sr (502-819 to 24-78 ppm) is recorded in the trachyte/trachyphonolite transition.

Major- and trace-element composition of the observed mineral phases is reported in the following section, with the only exception being clinopyroxene for which full description and discussion were presented in Fedele et al. (2009). Enclosing glass compositions were similarly

142 investigated in Fedele et al. (2009) and so they will be only briefly summarized below.
143 Compositional data are given in Tables 1, 2, 3, 4 and 5, completed by the Electronic Appendix.
144
145 Glasses
146 Glasses from BM trachyte samples are characterized by trachytic compositions with: 1) SiO_2 =
147 59.9-61.9 wt%, Na_2O = 2.73-4.71 wt%, K_2O = 8.17-9.40 wt% and P.I. = 072-092; 2) low MgO
148 (0.61-0.81 wt%) and CaO (2.17-2.54 wt%); 3) Mg# [Mg# = molar Mg/(Mg+Fe+Mn)] in the
149 range of 0.24-0.28; 4) relatively high abundances for strongly incompatible elements such as
150 LILE, (e.g., Rb, Cs, Ba, and Sr), LREE, HFSE (e.g., Zr and Nb); 5) very low Sc, V and Cr (Table
151 1). Primitive mantle-normalized (McDonough and Sun 1995) multi-element diagrams are LREE
152 enriched (La_N = 66.1-95.2, La_N/Sm_N = 4.0-5.3, La_N/Yb_N = 12.2-17.6) and nearly flat for HREE
153 (Ho_N/Yb_N = 0.98-1.32), with peaks at Th, U and Pb, and troughs at Sr and Ti (Fig. 3). Two
154 "anomalous" glass compositions have been observed within sample AI (one having a
155 trachyphonolitic composition), characterized by a relative Na_2O enrichment, FeO, MgO and CaO
156 depletion, slightly lower Mg#, higher REE, Y and HFSE and troughs at Sr, Ba and Eu.
157 Analyzed BM trachyphonolites have trachyphonolitic glasses that show higher Na_2O (5.23-
158 6.37 wt%), P.I. (0.86-0.97), REE, Y, HFSE and Pb and lower MgO (0.26-0.56 wt%), CaO (1.63-
159 2.42 wt%), K_2O (6.53-7.40 wt%), Mg# (0.12-0.23), Sc, V, Sr and Ba with respect to trachytic
160 glasses (Table 1). Primitive mantle-normalized patterns are LREE enriched (e.g., La_N = 126-253,
161 La_N/Yb_N = 8.21-16.5) and nearly flat in the HREE region, whith stronger LREE/MREE (e.g.,
162 La_N/Sm_N 4.31-6.99) and weaker MREE/HREE fractionation (Sm_N/Yb_N 1.91-2.79; Fig. 4) with
163 respect to glasses from trachytic samples. Normalized patterns also show marked troughs at Ba,
164 Sr and Eu. Trachyphonolitic glasses can be thus considered to represent slightly more
165 differentiated melts with respect to trachytic ones. Glasses from sample R show some chemical

166 variability pointing to slightly "transitional" compositions between trachytic and trachyphonolitic
167 glasses.

168

169 Feldspars

170 **Trachytes.** Plagioclase occurs as subhedral tabular phenocrysts/microphenocrysts, commonly
171 showing a turbid appearance (due to abundant glass inclusions) and corroded rims (Fig. 1a,b,c).
172 Analyzed crystals are bytownites ($An_{78-87}Ab_{11-19}Or_{1-5}$; Fig. 2) with moderate variability both in
173 major (e.g., Al = 1.76-1.87 apfu, Ca = 0.76-0.90 apfu, Na = 0.11-0.18 apfu; Table 2) and trace-
174 elements (e.g., Sr = 2424-3078 ppm, Ba = 100-219 ppm, Rb = 0.6-17 ppm, Pb = 5-7 ppm; Table
175 3). Primitive mantle-normalized incompatible element diagrams have peaks at Sr, Ba and Eu and
176 with very high Eu/Eu* [7.21-11.8, where $Eu/Eu^* = Eu_N/(Sm_N \times Gd_N)^{1/2}$] and the typical
177 LREE/MREE and LREE/HREE fractionation (Fig. 3).

178 Alkali feldspar crystals are large homogenous tabular/columnar sanidine phenocrysts, up to ~7
179 mm long (Fig. 1a,b,c) with a narrow compositional range ($An_{2-4}Ab_{12-16}Or_{80-86}$; Fig. 2) in both
180 major and trace-elements, except for Sr (basically 1023-2042 ppm; a analysis has 308 ppm), Ba
181 (597 up to >10000 ppm; a single has 112 ppm) and, less evidently, Rb (143-223 ppm; Tables 2
182 and 3). Similarly to plagioclases, primitive mantle-normalized diagrams for BM alkali feldspars
183 are markedly fractionated (Fig. 3), showing peaks at Rb, Ba, Sr and Eu and low HREE.

184 **Trachyphonolites.** Plagioclase is represented by subhedral-euhedral tabular microphenocrysts
185 (Fig. 1d,e,f). Two distinctive plagioclase types were observed: a bytownite ($An_{83-86}Ab_{14-16}Or_{0-1}$)
186 and an andesine-oligoclase ($An_{26-32}Ab_{59-62}Or_{10-13}$; Fig. 2). The calcic plagioclase, observed only
187 in sample B, matches the plagioclase of trachytic samples, with high Sr (>2200 ppm) and Ba
188 (~115 ppm) and low K_2O (~0.01 apfu) and incompatible elements (typically below or only barely
189 above the detection limits; Table 2 and 3). On the other hand, the Na-rich variety is remarkably

190 richer in LREE, while it has much lower Sr (176-303 ppm) and Ba (25-34 ppm). Primitive
191 mantle-normalized patterns for the two plagioclase types have similar shape, both slightly
192 LREE/HREE enriched and with peaks at LILE and Eu. The Ca-rich phenocrysts, still very similar
193 to the plagioclase of the trachytic samples, are systematically poorer in the most incompatible
194 elements (e.g., Th, La and Ce) and Pb, and have more evident peaks at Ba and Sr with respect to
195 the Na-rich ones, which show higher LREE and slightly higher Eu peaks (Eu/Eu* ~13.4; Fig. 4).
196 Alkali feldspar is the dominant phenocryst phase, represented by euhedral columnar
197 microphenocrysts ~1 mm long (Fig. 1d,e,f), occasionally up to 5-6 mm. Analyzed alkali feldspars
198 are sanidines with a homogeneous composition (i.e., $An_{3-4}Ab_{34-37}Or_{58-63}$), considerably poorer in
199 K (0.57-0.63 apfu) and richer in Na (0.33-0.37 apfu) with respect to their equivalents from BM
200 trachytes. Trace-element abundances are similarly homogeneous, characterized by lower Sr (157-
201 188 ppm) and Ba (270-309 ppm) and higher Rb (238-269 ppm), Pb (26-30 ppm) and LREE with
202 respect to sanidine from trachytes. Primitive mantle-normalized diagrams are quite similar to
203 those of alkali feldspars from BM trachytes, with less pronounced peaks at Ba, Sr and Eu, and
204 higher Rb, Cs and LREE (Fig. 4). With respect to coexisting plagioclases, alkali feldspars from
205 trachyphonolites are richer in Cs, Rb, Ba, Pb, Eu and Ti (the latter two with a lower extent) and
206 poorer in Sr and REE.
207
208 Opaque oxides
209 Opaque oxides occur as accessory small subhedral-euhedral microphenocrysts in both
210 trachytes and trachyphonolites (Fig. 1b,e), sometimes included in clinopyroxene and biotite
211 crystals. The opaques belong to the spinel s.s. and can be classified as Ti-magnetites (Fig. 5a),
212 characterized by higher Al_2O_3 and MgO (3.88-4.33 and 2.42-2.74 wt%, respectively) and lower
213 TiO_2 (5.68-5.78 wt%, ulvöspinel content ~17 mol%) in trachytes with respect to trachyphonolites

(Al_2O_3 = 1.93 wt%, MgO = 1.49 wt%, TiO_2 = 9.50 wt%, ulvöspinel content = 26.6 mol%; Table 4). Vanadium is typically enriched (1961-2398 ppm and 823 ppm, respectively for trachytes and trachyphonolites), whereas Cr (113-157 and 51 ppm), Zr (22-24 and 69 ppm), Nb (8-10 and 51 ppm) and Sc (8-9 and 4 ppm) are low. Other trace-element contents are typically very low, most of them being below the detection limits (Table 5; Fig. 6).

Biotite

Trioctahedral biotite mica crystals [according to the nomenclature of Rieder et al. (1999); Fig. 5b] have been observed and analyzed only in the trachytic samples, where they occur as sporadic euhedral microphenocrysts with the typical lamellar habit (Fig. 1a,b) and a characteristic brown to pale yellow pleochroism. Analyzed individuals show moderately high Mg# (~0.66) and TiO_2 (~4.8 wt%; Table 4) and generally very low trace-element concentrations (especially for Y and the REE, typically <0.1 ppm or even below the detection limits), with the exception of LILE (e.g., Rb = 294-307 ppm, Sr = 69-95 ppm, Ba = 2903-5275 ppm), V (426-486 ppm), HFSE (e.g., Zr ~22 ppm, Nb = 41-48 ppm, Ta = 1.68-1.85 ppm; Table 5) and Sc (~12 ppm), many of which have peaks in the primitive mantle-normalized diagrams of Fig. 7a.

Apatite

Apatite was observed only in trachyphonolitic sample I as very small microphenocrysts with prismatic habits. The apatite is relatively rich in Ca (9.96 apfu, almost completely filling the M1 and M2 sites) and F (3.83 wt%, *fluorapatite/hydroxyl-fluorapatite*) and poor in Si (0.17 apfu; Table 4), Y, Th, U and REE (e.g., Y = 1486 ppm, Th = 110 ppm, La = 3635 ppm, Ce = 7325 ppm; Table 5). Thus, the analyzed crystal approaches the composition of pure apatite end-member [i.e., $Ca_5(PO_4)_3(F,OH)$, with minor britholite silico-phosphate,

238 $(Ca,REE,Y,Th,U)_5(SiO_4,PO_4)_3(F,OH)$; Fig. 5c], and it can be classified as *fluorapatite/hydroxyl-*
239 *fluorapatite*. The primitive mantle-normalized pattern has a marked LREE/HREE- (La_N/Yb_N
240 ~38) and LREE/MREE- enrichment (La_N/Sm_N ~4.4), with troughs at Ba, Pb, Sr, Eu and V (Fig.
241 7b). Apatite is the main mineral repository of Th and U.
242
243 Discussion
244 The trace-element concentrations analyzed by LA-ICP-HRMS for mineral phases and
245 coexisting glasses within the studied BM samples were used for the calculation of mineral/liquid
246 partition coefficients for trachytic and trachyphonolitic systems. The reliability of such $^{Min/L}D$
247 values is obviously dependent on the effective attainment of equilibrium conditions. The overall
248 chemical homogeneity of both trachytic and trachyphonolitic glasses allows assuming they
249 reasonably represent the composition of the fractionating magma. However, a more detailed
250 inspection of both major- and trace-element glass composition showed some variability in
251 samples AI and R, possibly suggesting the persistence of local heterogeneities. Chemical
252 variability is particularly wide for trachytic sample AI (with glasses ranging from trachytic to
253 trachyphonolitic in composition), whereas it is less pronounced for trachyphonolite R (with only
254 glass analysis, R-3-VETROC, slightly deviating from the others in terms of lower Y, REE, Pb,
255 Th and U concentrations, more similar to the values of trachytic glasses). In the light of the above
256 observations, in order to correctly define the equilibrium partitioning and calculate $^{Min/L}D$ values:
257 • for BM trachytes, trachyphonolitic glass analyses from sample AI were discarded, whereas
258 trachytic glasses from the same sample were taken, given their similar composition with
259 respect to those from samples AN and C;

- for BM trachyphonolites, only the single anomalous glass analysis from sample R was discarded, whereas glass analyses from sample I were taken.

In the following sections the extent to which analyzed minerals satisfy criteria of phenocryst-matrix equilibrium is considered. It is worth noting here that the incorporation of trace-elements coming from the coexisting melts into a mineral structure is commonly ruled by the match in valence and ionic radius between the major-element cation and the trace-element(s) substituting after it. Lattice-site elastic-strain models are adopted to unravel the role of the crystal-chemical control on trace-element incorporation in minerals and their partitioning between solid and melt. In these models (Nagasawa 1966; Brice 1975) trace-elements are regarded as impurities introduced in a perfectly elastic and isotropic crystal lattice that minimise its perturbation by relaxing the adjacent sites and distributing the surplus elastic or electrostatic energy through the lattice. The equations of Beattie (1994) and Blundy and Wood (1994) describe the relationships among partition coefficients, ionic radii and ionic charges. Fedele et al. (2009) used the Blundy and Wood (1994) mathematical treatment to fit the partition coefficients of series of isovalent cations entering structure sites of clinopyroxene in equilibrium with BM trachyte-trachyphonolite melts. In principle, the same approach could be extended to the ${}^{Min/L}D$ of this study. However, the limited number of crystals suitable to measure equilibrium partitioning and the limited number of elements hosted by most of the mineral phases considered here makes the modelling of obtained ${}^{Min/L}D$ according to commonly adopted lattice-site elastic-strain models less reliable. Thus, the ${}^{Min/L}D$ are compared with those predicted according to semi-empirical parameterizations or straightforwardly to literature data.

Plagioclase

Assessment of equilibrium. Several lines of evidence indicate that Ca-rich bytownitic plagioclase crystals in trachytic samples cannot be regarded as the crystallization product of a trachytic-trachyphonolitic melt. Rather, they more likely represent a xenocryst phase. First of all, petrographic evidence of textural disequilibrium is provided by the occurrence of corroded rims (Fig. 1a,b,c,d), which suggest crystal/melt re-equilibration reactions. Secondly, the chemistry of these plagioclases plots on the less differentiated end of the entire Campi Flegrei trend (see Fig. 2), in the compositional field of crystals in equilibrium with the less evolved shoshonitic basalts, shoshonites and latites (e.g., Armienti et al. 1983; Beccaluva et al. 1990; D'Antonio and Di Girolamo 1994; Fedele et al. 2006). These observations are in keeping with previous studies that documented for BM trachytes-phonolites and other Campi Flegrei evolved rocks the presence of xenocryst Mg-rich clinopyroxene crystals originally equilibrated in less evolved, nearly-primitive melts and the concurrent occurrence of (xenocryst) Ca-rich and (equilibrium) Na-rich (labradorite-andesine, An_{35-55}) plagioclase (Melluso et al. 1995, 2012; Orsi et al. 1995; Civetta et al. 1997; de Vita et al. 1999; Pappalardo et al. 2002, 2008; Fulignati et al. 2004; Fedele et al. 2008, 2009). Chemical disequilibrium is also confirmed by the significantly lower An contents (i.e., An_{43-51} and An_{52-55} for dry and wet magmatic systems, respectively) of putative plagioclase in equilibrium with host BM trachytes according to the equation of Bédard (2006). On this basis, the analyzed plagioclases from the studied BM trachytes cannot be in chemical equilibrium with the coexisting glass and, consequently, were not used for the calculation of $^{Pl/L}D$ for trachytic liquids. Similar considerations indicate that the Ca-rich plagioclase is not in equilibrium with BM trachyphonolites. Only Na-rich plagioclase meets textural and chemical requirements to be regarded as a liquidus phase for Campi Flegrei evolved trachytic melts (Fig. 2). Accordingly, its composition approaches that calculated assuming equilibrium with host trachyphonolitic melt

(i.e., An_{23-38} and An_{43-51} for dry and wet magmatic systems, respectively) according to the equation of Bédard (2006). The composition of this plagioclase was therefore used for the calculation of trace-element partition coefficients by dividing average trace-element abundances for minerals and coexisting glasses, as reported in Table 6.

Calculated $^{Pl/L}D$ values and comparison with literature data. The only compatible elements are Sr ($^{Pl/L}D$ values ranging from 9.5 to 15), Ba (1.5-2.6) and Eu (1.1-1.4), whereas all the other trace-elements show a strongly (e.g., LILE, HFSE, M-HREE, Y and Ti, with $^{Pl/L}D \leq 0.08$) to moderately (e.g., Sc = 0.42-0.48, Pb = 0.20-0.24, La = 0.17-0.20, Ce = 0.10-0.12) incompatible behaviour (Fig. 8a). The presented $^{Pl/L}D$ values are basically consistent with data obtained using the theoretical model of Bédard (2006), based on plagioclase anorthite molecular values and MgO concentration of supposed equilibrium melt, thus supporting the hypothesis of plagioclase/trachyphonolite equilibrium (Fig. 8b). The fit is particularly good for the key elements Rb, Ba, Sr and Eu and acceptable for LREE. On the other hand, partition coefficients for Th, U, HFSE (Ti excluded) and HREE are quite overestimated, although still displaying incompatible behaviour. Fig. 8b also shows the results of the application of the Bédard (2006) model to the Ca-rich plagioclase of both BM trachytes and trachyphonolites. The mismatch in the calculated $^{Pl/L}D$ values for the key elements, especially Sr and Eu resulting strongly incompatible, is a further evidence for the xenocryst nature of such plagioclase.

The literature data for Campi Flegrei trachytes and trachyphonolites (Table 6) show several differences with the present dataset. Villemant (1988) measured $^{Feldspar/L}D$ in trachyte-trachyphonolite melts, obtaining values that are significantly higher for Ba (9.5 to 16.6) and Rb (0.52-0.97) and markedly lower for Sr (2-6.6) and Eu (0.85-1.17). The contrasting results mainly arise from the different sampling and analytical solutions. The data of Villemant (1988) data were obtained by INAA (Instrumental Neutron Activation Analysis) on mineral separates and

associated groundmass. Such a bulk technique is not able to avoid sampling bias related to the presence of either phases not completely equilibrated with the coexisting melt and/or occasional glass contamination, differently from *in situ* microanalytical investigations carried out by LA-ICP-HRMS (Fedele et al. 2009). Presumably, feldspar separates analysed by Villemant (1988) included alkali feldspars and, probably, xenocryst Ca-rich plagioclase. This clearly results in a wide broadening of $^{Feldspar/L}D$ values. The higher K_2O contents of the former facilitate the entrance of Ba and Rb in the crystal lattice, while hampering that of Sr, which, in contrast better enters Ca-rich plagioclase.

Compared to the $^{Pl/L}D$ values reported here, Pappalardo et al. (2008) obtained lower values for Ba (0.90 and 0.05 for trachyphonolites and trachytes, respectively), Sr (1.40 and 7.80 for trachytes and trachyphonolites, respectively) and Eu (0.90-0.80). It is to notice that he dataset of Pappalardo et al. (2008), though restricted to only seven trace-elements, was obtained by SIMS (Secondary Ions Mass Spectrometry), a microanalytical technique that furnishes *in-situ* chemical information more comparable with that obtained by LA-ICP-HRMS. However, the lack of an accurate assessment that equilibrium conditions were attained led the authors themselves to consider their values compositional ratios rather than effective partition coefficients. Literature data for other trace-elements are too scattered and $^{Pl/L}D$ values generally too low to allow a systematic comparison with the present dataset, even though a generally stronger correspondence can be easily envisaged, as it is the case of LREE and MREE in trachyphonolitic systems.

Finally, as regards the comparison with $^{Pl/L}D$ for other highly-differentiated systems (Table 6), the following observations can be reported: (a) phonolites display similar $^{Pl/L}D$ for all the trace-elements, although basically displaced to higher values, especially for the compatible Ba (1.73-7.33), Sr (11.7-49.8) and Eu (0.99-2.18); (b) with the exception of systematically lower $^{Pl/L}D_{Sr}$ (0.94-4.2), partition coefficients for sodic trachytic liquids are generally largely variable with

354 respect to those for potassic BM trachyphonolites (e.g., Eu and Ba range from incompatible to
355 strongly compatible; (c) rhyolites generally have wide $^{Pl/L}D$ ranges for the key elements,
356 displaying higher values with respect to BM trachyphonolites (i.e., $^{Pl/L}D_{Rb}$ = 0.06-0.76, $^{Pl/L}D_{Eu}$ =
357 2.0-7.9, $^{Pl/L}D_{Pb}$ = 0.27-2.2), whereas Sc is markedly more incompatible (0.01-0.06); (d) high
358 silica rhyolites have largely variable $^{Pl/L}D_{Ba}$ (1.0-19.55), generally lower $^{Pl/L}D_{Sr}$ (4.04-13.1) and
359 higher $^{Pl/L}D_{Eu}$ (3.65-5.62) and $^{Pl/L}D_{Pb}$ (0.35-0.97) compared to the corresponding values reported
360 here for BM trachyphonolites.
361
362 Alkali feldspar
363 **Assessment of equilibrium.** The textural evidence and the homogeneous major element
364 composition (well within the literature range for alkali feldspars from Campi Flegrei evolved
365 rocks; Fig. 2) confirm that alkali feldspar crystals from BM are in equilibrium with coexisting
366 glasses. Nevertheless, some variability that may be source of uncertainty in the calculation of
367 appropriate $^{Kfs/L}D$ values is observed at the trace-element scale; this is the case, for instance, of
368 Ba, Sr and Rb. This variability likely reflects the effects of slight differences in the fractionation
369 trend that led the melt to be progressively Ba- and Sr-poorer. On this basis, it seems reasonable to
370 argue that the crystals showing the strongest Ba and Sr enrichment (namely, C-1-SAN40-7 and
371 C-1-SAN40-3 and AI-4-SAN15-4, from samples C and AI, respectively) were segregated from
372 slightly less evolved liquids (see also the lower Rb, Pb and L-MREE abundances), and therefore
373 they are unsuitable for the calculation of $^{Kfs/L}D$ values. Similarly, the trace-element composition
374 of sanidine AN-4-SAN11-1 from trachyte AN is virtually identical to that of the other sanidine
375 crystals from BM trachytes (Table 3), but it is characterised by significantly lower Ba (112 ppm)
376 and Sr (308 ppm) contents (possibly due to analytical issues) to assume complete equilibrium.
377 This sample was therefore discarded. In virtue of their notably smaller Ba and Sr variability, the

remaining sanidine crystals were assumed to better represent trachytic liquidus phases. Their compositions were therefore used in the calculation of $^{Kfs/L}D$ values reported in Table 7.

Calculated $^{Kfs/L}D$ values and relevant changes from trachytes to trachyphonolites. With $^{Kfs/L}D$ values in the range of 2.5-5.4 and 2.5-3.1, Ba and Sr, respectively, are the only compatible elements in trachytes (Fig. 9). Europium oscillates from slightly incompatible to slightly compatible (0.87-1.2), whereas Rb and Pb behave as slightly/moderately incompatible elements (0.70-0.81 and 0.47-0.57, respectively). Finally, $^{Kfs/L}D_{Ti}$ and $^{Kfs/L}D_{Sc}$ are respectively between 0.13 and 0.24 and between 0.35 and 0.54, whereas the remaining trace-elements (mainly LREE) show a strongly incompatible behaviour ($^{Kfs/L}D \leq 0.1$).

The sanidine crystals in trachyphonolites have a homogeneous K_2O-poorer and Na_2O-richer composition that is consistent with Campi Flegrei literature data as for both the compositional range and the chemical changes at the transition from trachytes to trachyphonolites (Fig. 2). The assessment of the attainment of crystal/liquid equilibrium is thus more straightforward, and the calculation of $^{Kfs/L}D$ more reliable (Table 7). Compared to trachytes, trachyphonolites are characterized by higher $^{Kfs/L}D$ values for Ba (16-21), Sr (7.5-8.8) and, less markedly, Eu (1.2-1.4), whereas the remaining trace-elements are characterized by a slight decrease of $^{Kfs/L}D$ values (still showing a moderately to strongly incompatible behaviour; Fig. 9). Rubidium and Pb are moderately incompatible (0.50-0.60 and 0.34-0.45, respectively), both recording a slight decrease of $^{Kfs/L}D$ values with respect to trachytes.

The general decrease of $^{Kfs/L}D$ values for incompatible elements at the trachyte-trachyphonolite transition (extended also to $^{Cpx/L}D$ values; Fedele et al. 2009) is possibly related to a decrease of melt polymerization, as observed by White et al. (2003) for the transition from alkaline to peralkaline systems (i.e., with P.I. ≥1.0). In the case of Rb, the decrease of $^{Kfs/L}D$ seems also related to the lower presence of the orthoclase molecule in the alkali feldspar, given the great

geochemical similarity of Rb and K (both in terms of charge and size; e.g., Mahood and Stimac 1990, White 2003). A similar linear relation between Or content and $^{Kfs/L}D_{Rb}$ has been previously documented for peralkaline (White et al. 2003) and peraluminous silicic systems (Icenhower and London 1996).

In contrast, the partitioning of compatible elements in alkali feldspar seems barely affected by variations in melt polymerization (White et al. 2003). Thus, the observed increase of $^{Kfs/L}D$ for Ba and Sr must be related to other causes. One possibility is that both elements substitute for Na in a Ca-poor alkali feldspar and, therefore, their partition coefficients increase as a consequence of the higher Ab content in the alkali feldspar of trachyphonolites. Again, a similar feature has been observed by White (2003) and White et al. (2003) for peralkaline systems. Finally, the mild increase of $^{Kfs/L}D_{Eu}$ with increasing degree of evolution cannot be simply explained, due to the concomitant occurrence of Eu^{2+} and Eu^{3+}. These latter can have variable, sometimes contrasting, behaviour as a function of the variations in the oxidation state, melt polymerization and lattice features. However, it is proposed that the slight increase of $^{Kfs/L}D_{Eu}$ can be the result of a dominant effect of Eu^{2+} (which is supposed to become more compatible in trachyphonolites, having the same ionic radius and charge of Sr) over Eu^{3+} (supposed to be more incompatible in trachyphonolites like Sm and Gd).

Comparison with literature data. Similarly to $^{Pl/L}D$, also $^{Kfs/L}D$ for Campi Flegrei trachyte-trachyphonolite melts show some major differences with literature datasets, particularly as for Ba and Sr. As for trachytic systems, both $^{Feldspar/L}D$ from Villemant (1988) and $^{Kfs/L}D$ from Pappalardo et al. (2008) show a much wider spectrum of values relative to those of this study (Table 7). The markedly lower $^{Feldspar/L}D_{Ba}$ (down to 1.13) and higher $^{Feldspar/L}D_{Sr}$ (up to 6.6) by Villemant (1988) are likely ruled by dominant Ca-rich plagioclase. In contrast, the notably higher $^{Feldspar/L}D_{Ba}$ values (up to 16.6) by Villemant (1988) and the wide range of $^{Kfs/L}D_{Ba}$ values (0.3 to

13) by Pappalardo et al. (2008) are probably the result of localized heterogeneities in the analyzed samples. As for trachyphonolites, our $^{Kfs/L}D$ are notably higher for Ba and only slightly higher for Sr and Eu, the latter being slightly incompatible according to Pappalardo et al (2008). As a whole, it is proposed that the observed differences result from the sampling and analytical issues previously discussed in the plagioclase section.

A comparison between present data and literature data for other evolved systems is shown in Table 7. The trachytes of White et al. (2003) display lower $^{Kfs/L}D_{Rb}$ (0.24-0.37), higher $^{Kfs/L}D_{Eu}$ (2.04-2.10) and largely variable $^{Kfs/L}D_{Ba}$ (1.11-12.74, quite within the range of the data presented here) and $^{Kfs/L}D_{Sr}$ (0.45-4.81, only barely comparable with present data for trachytes). Such differences are probably the effect of numerous factors, including variations in bulk-rock SiO_2 and P.I. (both influencing the degree of melt polymerization) and in crystal chemistry as well (White et al. 2003). As for sodic trachytes, $^{Kfs/L}D_{Ba}$ (5.2-5.9) roughly compares with that measured in BM trachytes, $^{Kfs/L}D_{Rb}$ is definitely lower (0.11-0.26), whereas $^{Kfs/L}D_{Sr}$ (3.6-10) and $^{Kfs/L}D_{Eu}$ (0.4-2.5) cover the entire range of the present dataset and even extends to higher values. Pantellerites and comendites (peralkaline rhyolites) are characterized by an overall decrese of partition coefficients for incompatible elements and Rb with respect to BM trachytes-trachyphonolites. This decline of $^{Kfs/L}D$ at the trachyte/pantellerite transition should be probably ascribed to a decrease of melt polymerization, as observed by Mahood and Stimac (1990) and White et al. (2003). In contrast, compatible elements display a broad range of $^{Kfs/L}D$, with values that are lower and higher relative to those for BM trachytes and typically lower compared to those for BM trachyphonolites (e.g., $^{Kfs/L}D_{Ba}$ = 0.66-10.35, $^{Kfs/L}D_{Sr}$ = 0.40-2.79). This probably reflects the influence of numerous interplaying factors in their partitioning (as mentioned above; see White et al. 2003). As for rhyolitic systems, LILE (e.g., $^{Kfs/L}D_{Rb}$ = 0.31-2.4, $^{Kfs/L}D_{Pb}$ = 0.99-4.1) and Eu (2-9.06) display higher partition coefficients, whereas Sr shows $^{Kfs/L}D$ values

intermediate between BM trachytes and trachyphonolites (i.e., 4.5-7.3) and Ba basically encompasses the range for analyzed trachytes and trachyphonolites (1-24). Finally, high-silica rhyolites show roughly similar, although widely variable, ${}^{Kfs/L}D_{Rb}$ (0.11-0.74) and ${}^{Kfs/L}D_{Ba}$ (1.0-20.9) with respect to BM trachytes and trachyphonolites, whereas ${}^{Kfs/L}D_{Sr}$, ${}^{Kfs/L}D_{Eu}$ and ${}^{Kfs/L}D_{Pb}$ are remarkably higher.

Ti-magnetite

Titanomagnetite crystals from both trachytes and trachyphonolites do not show any textural evidence for disequilibrium and display compositions that are well within the range reported for opaque oxides from Campi Flegrei evolved products (i.e., ulvöspinel contents basically between 16 and 29%, with only a few higher values in the range 40-62%; Fig. 5a). As a comparison, Ti-magnetite crystals in the slightly less evolved (latite-trachyte) pyroclastic rocks from the nearby Ischia district have slightly higher ulvöspinel (~35-46%), TiO_2 (10.4-15.6 wt%) and MgO contents (2.40-5.04 wt%) and lower FeOtot (72.1-77.9 wt%). The analyzed crystals can be reasonably considered as the direct product of segregation from their coexisting trachytic/trachyphonolitic glasses and therefore are used for the calculation of ${}^{Mt/L}D$ values, reported in Table 8.

The very low trace-element concentration of analyzed Ti-magnetite crystals is apparent from Fig. 10a, in which only Ti (${}^{Mt/L}D_{Ti}$ = 18-19 for trachytes, 25 for trachyphonolites) and V (${}^{Mt/L}D_{V}$ = 44-49 and 55) show a strongly compatible behaviour. Scandium varies from moderately compatible in trachytes (D_{Sc} = 1.7) to barely incompatible (0.96) in trachyphonolites. Interestingly, Sc is the only trace-element for which a clear decline in ${}^{Mt/L}D$ values can be observed as melt changes in composition from trachyte to trachyphonolite. Among the remaining trace-elements, only HFSE have ${}^{Mt/L}D$ above 0.1 (and typically ≤0.4; Fig. 10a). A general trend of

474 increasing compatibility of Ti and HFSE can be envisaged at the trachyte-trachyphonolite
475 transition, likely related to the increase of Ti and Fe/Mg and the concurrent decrease of Al. This
476 trend, along with evidence that $^{Mt/L}D_{Ti,V,Sc} > {}^{Mt/L}D_{HFSE}$ and $^{Mt/L}D_{Th,U} < 0.035$, are consistent with
477 results and related considerations reported by Nielsen et al (1994) for basic to intermediate
478 systems.

479 As a whole, strongly incompatible elements (e.g., LILE, LREE and MREE) are typically
480 below the detection limits in our dataset, whereas, a moderately incompatible to slightly
481 compatible behaviour is reported by Villemant (1988) for some of them (e.g., La, Eu and Tb;
482 Table 8). These high $^{Mt/L}D$ values are most probably due to unusually REE-rich contents that
483 reflect the presence of late-stage phase inclusions (e.g., apatite, zircon, rutile; see Nielsen et al.
484 1994). Differences in the adopted analytical techniques (see above) may also explain the strongly
485 compatible behaviour of Sc (with $^{Mt/L}D_{Sc}$ increasing from 3.80-7.95 to 9.70 at the
486 trachyte/trachyphonolite transition) measured by Villemant (1988).

487 Finally, large differences are observed between $^{Mt/L}D$ for trachytic-trachyphonolitic liquids and
488 those for other differentitated systems (Table 8). The most remarkable are reported in the
489 following: (a) phonolites display generally higher $^{Mt/L}D$ values (e.g., $^{Mt/L}D_U$ = 0.725, $^{Mt/L}D_{Ta}$ =
490 0.164-0.90, $^{Mt/L}D_{Sc}$ = 2.85-5.38); (b) in Na-trachytes Ta is compatible ($^{Mt/L}D_{Ta}$ = 0.28 or 1.13-
491 2.35) and Sc strongly compatible ($^{Mt/L}D_{Sc}$ = 1.88-10.42); (c) rhyolites and high-silica rhyolites
492 show higher $^{Mt/L}D$ values for all the trace-elements, including the more incompatible ones, some
493 of which can also turn to strongly compatible (e.g., $^{Mt/L}D_{Th}$ up to 13.1, $^{Mt/L}D_{Ta}$ up to 4.5, $^{Mt/L}D_Y$ up
494 to 3.21).

495

Biotite

The biotite crystals recovered in AI trachyte have a broadly similar composition, fully consistent with existing literature data for Campi Flegrei differentiates (i.e., Mg# = 0.61-0.74), as well as for those from similar rocks from Ischia (i.e., Mg# = 0.63-0.76; Fig. 5b). Only Ba and (less evidently) Sr and V exhibit a more marked chemical variability (Table 5), and so two sets of $^{Bt/L}D$ values were calculated (Table 9 and Fig. 10b), dividing the composition of each biotite crystal meeting the requirements of textural and chemical equilibrium by the average composition of coexisting trachytic glass.

The most compatible elements are, in order of decreasing $^{Bt/L}D$ values, Ti (14), V (8.8-10.0), Ba (5.7-10) and Sc (2.2-2.3). As for the other trace-elements, both LILE and HFSE range from strongly incompatible (e.g., Th, U, Pb, Sr, Zr, Hf), to moderately/barely incompatible (Cs, Ta), to slightly compatible (Rb, Nb). Differently from the other analyzed mineral phases, an overall good correspondence exists between $^{Bt/L}D$ values reported here and those measured by Villemant (1988), particularly for key elements such as Rb and Sr, but also for HFSE (e.g., Ta and Hf). Some discrepancies, such as the generally wider range of literature data (e.g., $^{Bt/L}D_{Sc}$ = 2.81-5.56, $^{Bt/L}D_{Ba}$ = 1.04-21.5) possibly result from crystal and/or glass compositional heterogeneities.

The present dataset is remarkably different from the previous ones reported for biotite in equilibrium with other evolved liquids, for which generally higher $^{Bt/L}D$ values for all the most relevant trace-elements are reported (Table 9). Partition coefficients for phonolitic systems are quite similar to those reported here for trachytes, with values that are basically slightly higher for Rb, lower for Ta (which is clearly incompatible) and one order of magnitude higher for Sc. Rhyolites and high-silica rhyolites are characterized by a notable increase of $^{Bt/L}D$ values for almost the entire spectrum of analyzed trace-elements, some of which display a particularly wide range (e.g., $^{Bt/L}D_{Cs}$ = 1.2-3.1, $^{Bt/L}D_{Rb}$ = 3.0-9.7, $^{Bt/L}D_{Ba}$ = 3.7-7.0).

520

521 Apatite

522 The few data available for Campi Flegrei trachyte-phonolite apatites display a wide
523 compositional variability, covering the range from near-pure apatite (similar to that reported here)
524 to terms rich in the britholite silico-phosphate component (i.e., Si+REE >6 apfu; Fig. 5c). It could
525 be hypothesized that the britholite-rich compositions are found in differentiated holocrystalline
526 trachytes and trachyphonolites (Melluso et al. 2012), as the extreme enrichment in lanthanides,
527 Th and U of the melt facilitates their entrance in the apatite-britholite crystal lattice, mainly at the
528 expense of CaO (whose abundance progressively decreases with magma evolution). In the Campi
529 Flegrei volcanic products such substitutions are associated with a decrease of F, which prefers to
530 enter fluorite and F-bearing Ca-Zr-disilicates (Melluso et al. 2012). A similar increase of Si,
531 LREE and Y (as well as of Fe) has been documented in the apatite crystals from Pantelleria at the
532 transition from trachytes to pantelleritic trachytes and pantellerites (Mahood and Stimac 1990). In
533 addition, Macdonald et al. (2013) documented the occurrence of both (relatively) early
534 crystallizing apatite and late crystallizing britholite in some Paleogene granites from Scotland and
535 Northern Ireland. Therefore, in light of the above considerations and in the absence of evidence
536 in favour of textural and/or chemical disequilibrium, the analyzed apatite crystal from
537 trachyphonolite sample I can be confidently considered as a liquidus phase. Calculated $^{Ap/L}D$ are
538 reported in Table 10 and in Fig. 10b.

539 Yttrium and REE are all strongly compatible, with $^{Ap/L}D$ values generally >20, except for the
540 heavier HREE, whose partition coefficients record a clear decrease with increasing atomic
541 number, from 17 (Er) to 7.8 (Lu). Highest values (≥30) are for MREE, consistently with both
542 theoretical and experimental data (see Prowatke and Klemme 2006). Large ion litophile elements
543 range from strongly/moderately incompatible (e.g., Pb, Ba, U) to moderately compatible (Th), up

to strongly compatible (Sr), whereas HFSE are all strongly incompatible (e.g., $^{Ap/L}D_{Ti}$ = 0.05; concentrations for all the other HFSE are below the detection limits) and and V is compatible ($^{Ap/L}D_V$ = 2.0). The latter can be explained by the ordering of V at Z site, in substitution of P (e.g., Pan and Fleet 2002).

Up to the present study, the only $^{Ap/L}D$ literature data available for apatite/evolved liquid equilibria refer to more than 20 year-old studies (see Table 9). The dataset of Prowatke and Klemme (2006) is not considered here because it refers to partitioning between apatite and synthetic silicate melts of less evolved composition (approximately ranging from basalt to andesite) at high *P* and *T* conditions (1.0 GPa and 1250 °C). As a whole, an overall good correspondence is observed with literature data for apatite/phonolite equilibrium. REE show a trend of increasing compatibility from LREE to MREE (e.g., $^{Ap/L}D_{La}$ = 14.4, $^{Ap/L}D_{Nd}$ = 54.3, $^{Ap/L}D_{Eu}$ = 102) followed by a reversal to lower values for HREE (e.g., $^{Ap/L}D_{Lu}$ = 3.69), with values significantly lower for LREE and HREE and markedly higher for MREE relative to those of this study. Similar observations can be made for sodic trachytes and pantellerites, which basically mimic the general trend observed in this study although their $^{Ap/L}D$ are generally higher, particularly for U and LREE. Finally, data for granitic systems indicate a much higher compatibility of HREE with respect to LREE, differently from evidence for Campi Flegrei trachyphonolites and the other evolved systems discussed above.

Implications

The present study provides a new dataset of partition coefficients for plagioclase, alkali feldspar, Ti-magnetite, biotite and apatite equilibrated with trachytic-trachyphonolitic potassic systems. The new set of $^{Min/L}D$ values has been obtained thanks to preliminary petrographic observations that suggested suitable textural conditions (i.e., glassy texture, low to moderate

568 phenocryst load) and the adoption of *in situ* microanalytical techniques that confirmed chemical
569 equilibrium between the analyzed mineral phases and coexisting melts.

570 Analyzed plagioclases include both Na- and Ca-rich terms, with only the former having
571 equilibrated with trachyphonolitic liquids, whereas the latter formed from less evolved melts
572 (possibly shoshonitic basalt). $^{Pl/L}D$ calculated for Na-rich terms are characterised by high values
573 for Sr, Ba and Eu. A marked increase of $^{Kfs/L}D$ for the compatible elements Ba, Sr (and Eu that
574 varied from slightly incompatible to slightly compatible in trachytes) and a clear (though small)
575 decrease of the remaining trace-elements (all incompatible at various extent) characterize the
576 transition from trachytes to trachyphonolites.

577 As regards Ti-magnetite, Ti, V and Sc are compatible elements in evolved trachytic-
578 trachyphonolitic systems, as broadly expected. A systematic decrease of $^{Mt/L}D$ values (with the
579 only exception of $^{Mt/L}D_{Sc}$) is observed at the transition from trachytes to trachyphonolites. The
580 highest $^{Bt/L}D$ values for trachytic liquids were calculated for Ti, Ba and Sc, whereas the remaining
581 HFSE and LILE show a variable partitioning behaviour (from strongly, moderately and slightly
582 incompatible to slightly compatible). The REE are strongly incompatible elements.
583 Apatite/trachyphonolite partition coefficients are high for Sr, Y and REE (the latter with $^{Ap/L}D$
584 values up to ~40), very low for HFSE and largely variable for the remaining LILE.

585 The comparison with the few sets of $^{Min/L}D$ available in literature for similar systems revealed
586 significant differences for the main trace-elements entering in the crystal lattice of the analyzed
587 mineral phases. Such discrepancies are possibly related to the different analytical methods (i.e., LA-
588 ICP-HRMS vs. INAA) and/or to the lack of an accurate evaluation of the attainment of equilibrium
589 conditions, thus confirming the importance of a preliminary sample selection and the adoption of *in*
590 *situ* microanalytical techniques. On the other hand, the differences observed between our $^{Min/L}D$ and

591 those for other differentiated systems, although in part related to the heterogeneity of the datasets
592 available for comparative purposes, stress out once again the need that each system must be
593 separately considered (Mahood and Stimac 1990, White et al. 2003, Fedele et al. 2009). The
594 different physical (T, P, fO_2, degree of polymerization) and chemical parameters (major element
595 content, degree of peralkalinity), as well as changes in mineral chemistry and in fractionating
596 mineral assemblage plus various kinetic effects (e.g., growth rate) can play a great influence on the
597 mineral/liquid partitioning and need to be adequately addressed.

598 It should be finally stressed that the determination of mineral/liquid partition coefficients for
599 highly evolved systems such as those investigated here can significantly improve the understanding
600 of magma evolution processes. As huge silica- and alkali-rich magma reservoirs are commonly
601 characterized by explosive eruptions (e.g., Mason et al. 2004 and references therein), a detailed
602 knowledge and modelling of the magmatic evolution can also contribute to a correct evaluation of
603 the volcanic hazard and related risks.

604

605 Acknowledgements

606 The authors wish to thank Marcello Serracino for help and assistance during EMP micronalyses.
607 Financial support was provided by LR N.5 (to L.F.), Fondi Ateneo 2012, 2013 and MIUR PRIN
608 2010 20107ESMX9_001 (to M.L.), PRIN 2003 (to L.M.) and LR N.5 CUP E64G08000050003
609 (to V.M.) grants. Official revisions from John C. White (Eastern Kentucky University) and an
610 anonymous reviewer significantly improved the quality of the manuscript. Careful editorial
611 handling from Associate Editor Paul B. Tomascak was greatly appreciated.

612

References

Armienti, P., Barberi, F., Bizouard, H., Clocchiatti, R., Innocenti, F., Metrich, N., Rosi, M., and Sbrana, A. (1983) The Phlegrean Fields: magma evolution within a shallow chamber. Journal of Volcanology and Geothermal Research, 17, 289-311.

Bacon, C.R., and Druitt, T.H. (1988) Compositional evolution of the zoned calcalkaline magma chamber of Mt. Mazama, Crater Lake, Oregon. Contributions to Mineralogy and Petrology 98, 224-256.

Beattie, P. (1994) Systematics and energetics of trace-element partitioning between olivine and silicate melts: Implications for the nature of mineral/melt partitioning. Chemical Geology, 117, 57-71.

Beccaluva, L., Di Girolamo, P., Morra, V., and Siena, F. (1990) Phlegraean Fields volcanism revisited: A critical re-examination of deep eruptive systems and magma evolutionary processes. Neues Jahrbuch fur Geologie und Paläontologie Monatshefte, 5, 257-271.

Bédard, J.H. (2006) Trace element partitioning in plagioclase feldspar. Geochimica et Cosmochimica Acta, 70, 3717-3742.

Blundy, J., and Wood, B. (1994) Prediction of crystal–melt partition coefficients from elastic moduli. Nature, 372, 452-454.

Brice, J.C. (1975) Some thermodynamic aspects of the growth of strained crystals. Journal of Crystal Growth, 28, 249-253.

Carmichael, I.S.E. (1967) The iron-titanium oxides of salic volcanic rocks and their associated ferromagnesian silicates. Contributions to Mineralogy and Petrology, 14, 36-64.

Civetta, L., Orsi, G., Pappalardo, L., Fisher, R.V., Heiken, G., and Ort, M. (1997) Geochemical zoning, mingling, eruptive dynamics and depositional processes - the Campanian Ignimbrite, Campi Flegrei caldera, Italy. Journal of Volcanology and Geothermal Research, 75, 183-219.

D'Antonio, M., and Di Girolamo, P. (1994) Petrological and geochemical study of mafic shoshonitic volcanics from Procida-Vivara and Ventotene Islands. Acta Volcanologica, 5, 69-80.

Deino, A.L., Orsi, G., de Vita, S., and Piochi, M. (2004) The age of the Neapolitan Yellow Tuff caldera-forming eruption (Campi Flegrei caldera – Italy) assessed by $^{40}Ar/^{39}Ar$ dating method. Journal of Volcanology and Geothermal Research, 133, 157-170.

De La Roche, H., Leterrier, P., Grandclaude, P., and Marchal, E. (1980) A classification of volcanic and plutonic rocks using R1-R2 diagram and major element analyses. Its relationships with current nomenclature. Chemical Geology, 29, 183-210.

de Vita, S., Orsi, G., Civetta, L., Carandente, A., D'Antonio, M., Deino, A., di Cesare, T., Di Vito, M.A., Fisher, R.V., Isaia, R., Marotta, E., Necco, A., Ort, M., Pappalardo, L., Piochi, M., and Southon, J. (1999) The Agnano-Monte Spina eruption (4100 years BP) in the restless Campi Flegrei caldera (Italy). Journal of Volcanology and Geothermal Research, 91, 269-301.

De Vivo, B., Rolandi, G., Gans, P.B., Calvert, A., Bohrson, W.A., Spera, F.J., and Belkin, H.E. (2001) New constraints on the pyroclastic eruptive history of the Campanian Volcanic Plain (Italy). Mineralogy and Petrology, 73, 47-65.

Di Girolamo, P., Melluso, L., Morra, V., and Secchi, F.A.G. (1995) Evidence of interaction between mafic and differentiated magmas in the youngest phase of activity at Ischia island (Italy). Periodico di Mineralogia, 64, 393-411.

D'Orazio, M., Armienti, P., and Cerretini, S. (1998) Phenocryst/matrix trace-element partition coefficients for hawaiite-trachyte lavas from the Ellittico volcanic sequence (Mt. Etna, Sicily, Italy). Mineralogy and Petrology, 64, 65-88.

D'Oriano, C., Poggianti, E., Bertagnini, A., Cioni, R., Landi, P., Polacci, M., and Rosi, M. (2005) Changes in eruptive style during the A.D. 1538 Monte Nuovo eruption (Phlegrean Fields, Italy): the role of syn-eruptive crystallization. Bulletin of Volcanology, 67, 601-621.

Ewart, A., and Griffin, W.L. (1994) Application of proton-microprobe data to trace-element partitioning in volcanic rocks. Chemical Geology, 117, 251-284.

Fedele, L., Morra, V., Perrotta, A., and Scarpati, C. (2006) Volcanological and geochemical features of the products of the Fiumicello eruption, Procida island, Campi Flegrei (southern Italy). Periodico di Mineralogia, 75, 43-72.

Fedele, L., Scarpati, C., Lanphere, M., Melluso, L., Morra, V., Perrotta, A., and Ricci, G. (2008) The Breccia Museo formation, Campi Flegrei, southern Italy: geochronology, chemostratigraphy and relationship with the Campanian Ignimbrite eruption. Bulletin of Volcanology, 70, 1189-1219.

Fedele, L., Zanetti, A., Morra, V., Lustrino, M., Melluso, L., and Vannucci, R. (2009) Insights on the clinopyroxene/liquid trace element partitioning in natural trachyte-trachyphonolite systems: an EMP/LA-ICP-MS case study from Campi Flegrei (southern Italy). Contributions to Mineralogy and Petrology, 158, 337-356.

Fowler, S.J., Spera, F.J., Bohrson, W.A., Belkin, H.E., and De Vivo, B. (2007) Phase equilibria constraints on the chemical and physical evolution of the Campanian Ignimbrite. Journal of Petrology, 48, 459-493.

Fulignati, P., Marianelli, M., Proto, M., and Sbrana, A. (2004) Evidences for disruption of a crystallizing front in a magma chamber during caldera collapse: an example from the Breccia Museo unit (Campanian Ignimbrite eruption, Italy). Journal of Volcanology and Geothermal Research, 133, 141-155.

Ghiara, M.R., Lirer, L., and Munno, R. (1979) Mineralogy and geochemestry of the "low-potassium series" of the Campania volcanics (South Italy). Chemical Geology, 26, 29-49.

Icenhower, J., and London, D. (1996) Experimental partitioning of Rb, Cs, Sr and Ba between alkali feldspar and peraluminous melt. American Mineralogist, 81, 719-734.

Icenhower, J.P., and London, D. (1997) Partitioning of flourine and chlorine between biotite and granitic melt: experimental calibration at 200 MPa H_2O. Contributions to Mineralogy and Petrology 127, 17-29.

Leeman, W.P., and Phelps, D.W. (1981) Partitioning of rare earths and other trace elements between sanidine and coexisting volcanic glass. Journal of Geophysical Research, 86, 10193-10199.

Lemarchand, F., Villemant, B., and Calas, G. (1987) Trace element distribution coefficients in alkaline series. Geochimica et Cosmochimica Acta, 51, 1071-1081.

Lustrino, M., Duggen, S., and Rosenberg, C.L. (2011) The Central-Western Mediterranean: Anomalous igneous activity in an anomalous collisional tectonic setting. Earth-Science Reviews, 104, 1-40.

Macdonald, R., Bagiński, B., Dzierżanowski, P., and Jokubauskas P. (2013) Apatite-supergroup minerals in UK Palaeogene granites: composition and relationship to host-rock composition. European Journal of Mineralogy, 25, 461-471.

Mahood, G.A., and Hildreth, W. (1983) Large partition coefficients for trace elements in high-silica rhyolites. Geochimica et Cosmochimica Acta, 47, 11-30.

Mahood, G.A., and Stimac, J.A. (1990) Trace-element partitioning in pantellerites and trachytes. Geochimica et Cosmochimica Acta, 54, 2257-2276.

Mason, B.G., Pyle, D.M., and Oppenheimer, C. (2004) The size and frequency of the largest explosive eruptions on Earth. Bulletin of Volcanology, 66, 735-748.

McDonough, W.F., and Sun, S.-s. (1995) The composition of the Earth. Chemical Geology, 120, 223-253.

Melluso, L., Morra, V., Perrotta, A., Scarpati, C., and Adabbo, M. (1995) The eruption of the Breccia Museo (Campi Flegrei, Italy): Fractional crystallization processes in a shallow, zoned magma chamber and implications for the eruptive dynamics. Journal of Volcanology and Geothermal Research, 68, 325-339.

Melluso, L., de' Gennaro, R., Fedele, L., Franciosi, L., and Morra, V. (2012) Evidence of crystallization in residual, Cl-F-rich, agpaitic, trachyphonolitic magmas and primitive Mg-rich basalt-trachyphonolite interaction in the lava domes of the Phlegrean Fields (Italy). Geological Magazine, 149, 532-550.

Miller, C., Zanetti, A., Thöni, M., and Konzett, J. (2007) Eclogitisation of gabbroic rocks: Redistribution of trace elements and Zr in rutile thermometry in an Eo-Alpine subduction zone (Eastern Alps). Chemical Geology, 239, 96-123.

Morra, V., Calcaterra, D., Cappelletti, P., Colella, A., Fedele, L., de' Gennaro, R., Langella, A., Mercurio, M., and de' Gennaro, M. (2010) Urban geology: relationships between geological setting and architectural heritage of the Neapolitan area. In M. Beltrando, A. Peccerillo, M. Mattei, S. Conticelli, and C. Doglioni, Eds, Geology of Italy. Journal of the Virtual Explorer, 36, paper 26. doi:10.3809/jvirtex.2010.00261.

Nagasawa, H. (1966) Trace element partition coefficient in ionic crystals. Science, 152, 769-771.

Nagasawa, H. (1970) Rare earth concentrations in zircon and apatite and their host dacite and granites. Earth and Planetary Science Letters, 9, 359-364.

Nagasawa, H. (1973) Rare-earth distribution in alkali rocks from Oki-Dogo Island, Japan. Contributions to Mineralogy and Petrology, 39, 301-308.

729 Nash, W.P., and Crecraft, H.R. (1985) Partition coefficients for trace elements in silicic magmas.
730 Geochimica et Cosmochimica Acta, 49, 2309-2322.
731 Nielsen, R.L., Forsythe, L.M., Gallahan, W.E., and Fisk, M.R. (1994) Major- and trace-element
732 magnetite-melt equilibria. Chemical Geology, 117, 167-191.
733 Orsi, G., Civetta, L., D'Antonio, M., Di Girolamo, P., and Piochi, M. (1995) Step-filling and
734 development of a three-layer magma chamber: the NYT case history. Journal of Volcanology
735 and Geothermal Research, 67, 291-312.
736 Pan, Y., and Fleet, M.E. (2002) Compositions of the apatite-group minerals: substitution
737 mechanisms and controlling factors. Reviews in Mineralogy and Geochemistry, 48, 13-49.
738 Pappalardo, L., Civetta, L., de Vita, S., Di Vito, M., Orsi, G., Carandente, A., and Fisher, R.V.
739 (2002) Timing of magma extraction during the Campanian Ignimbrite eruption (Campi Flegrei
740 Caldera). Journal of Volcanology and Geothermal Research, 114, 479-497.
741 Pappalardo, L., Ottolini, L., and Mastrolorenzo, G. (2008) The Campanian Ignimbrite (southern
742 Italy) geochemical zoning: insight on the generation of a super-eruption from catastrophic
743 differentiation and fast withdrawal. Contributions to Mineralogy and Petrology, 156, 1-26.
744 Pearce, N.J.G., Perkins, W.T., Westgate, J.A., Gorton, M.P., Jackson, S.E., Neal, C.R., and
745 Chenery, S.P. (1996) A compilation of new and published major and trace element data for
746 NIST SRM 610 and NIST SRM 612 glass reference materials. Geostandards Newsletter, 21,
747 115-144.
748 Perrotta, A., and Scarpati, C. (1994) The dynamics of the Breccia Museo Eruption (Campi
749 Flegrei Italy) and the significance of spatter clasts associated with lithic breccias. Journal of
750 Volcanology and Geothermal Research, 59, 335-355.

Perrotta, A., Scarpati, C., Luongo, G., and Morra, V. (2006) The Campi Flegrei caldera boundary in the city of Naples. In B. De Vivo, Ed., Volcanism in the Campania Plain: Vesuvius, Campi Flegrei and Ignimbrites. Developments in Volcanology, 9, p 85-96. Elsevier, Amsterdam.

Piochi, M., Civetta, L., and Orsi, G. (1999) Mingling in the magmatic system of Ischia (Italy) in the past 5 ka. Mineralogy and Petrology, 66, 227-258.

Piochi, M., Mastrolorenzo, G., and Pappalardo, L. (2005) Magma ascent and eruptive processes from textural and compositional features of Monte Nuovo pyroclastic products, Campi Flegrei, Italy. Bulletin of Volcanology, 67, 663-678.

Poli, S., Chiesa, S., Gillot, P.-Y., Gregnanin, A., and Guichard, F. (1987) Chemistry versus time in the volcanic complex of Ischia (Gulf of Naples, Italy): evidence of successive magmatic cycles. Contributions to Mineralogy and Petrology, 95, 322-335.

Prowatke, S., and Klemme, S. (2006) Trace element partitioning between apatite and silicate melts. Geochimica et Cosmochimica Acta, 70, 4513-4527.

Rieder, M., Cavazzini, G., D'yankonov, Y.S., Gottardi, G., Giggenheim, S., Koval, P.V., Müller, G., Neiva, A.M.R., Radoslovich, E.W., Robert, J.-L., Sassi, F.P., Takeda, H., Weiss, Z., and Wones, D.R. (1999) Nomencalture of the micas. Mineralogical Magazine, 63, 267-279.

Scarpati, C., Cole, P., and Perrotta, A. (1993) The Neapolitan Yellow Tuff – A large volume multiphase eruption from Campi Flegrei, Southern Italy. Bulletin of Volcanology, 55, 343-356.

Stormer, J.C. (1983) The effect of recalculation on estimates of temperature and oxygen fugacity from analyses of multicomponent iron-titanium oxides. American Mineralogist, 68, 586-594.

Streck, M.J., and Grunder, A.L. (1997) Compositional gradients and gaps in high-silica rhyolites of the Rattlesnake Tuff, Oregon. Journal of Petrology, 38, 133-163.

Stix, J., and Gorton, M.P. (1990) Variations in trace element partition coefficients in sanidine in the Cerro Toledo Rhyolite, Jemez Mountains, New Mexico: Effects of composition, temperature and volatiles. Geochimica et Cosmochimica Acta, 54, 2697-2708.

Villemant, B. (1988) Trace element evolution in Phlegreaen Fields (central Italy): fractional crystallization and selective enrichment. Contributions to Mineralogy and Petrology, 98, 169-183.

Watson, E.B., and Green, T.H. (1981) Apatite/liquid partition coefficients for the rare earth elements and strontuim. Earth and Planetary Science Letters, 56, 405-421.

White, J.C. (2003) Trace-element partitioning between alkali feldspar and peralkalic quartz trachyte to rhyolite magma. Part II: Empirical equations for calculating trace-element partition coefficients of large-ion lithophile, high field-strength and rare-earth elements. American Mineralogist, 88, 330-337.

White, J.C., Holt, G.S., Parker, D.F., and Ren, M. (2003) Trace-element partitioning between alkali feldspar and peralkalic quartz trachyte to rhyolite magma. Part I: Systematics of trace-element partitioning. American Mineralogist, 88, 316-329.

Wörner, G., Beusen, J.-M., Duchateau, N., Gijbels, R., and Schmincke, H.-U. (1983) Trace element abundances and mineral/melt distribution coefficients in phonolites from Laacher See Volcano (Germany). Contributions to Mineralogy and Petrology, 84, 152-173.

Figure captions

Figure 1. Thin section microphotographs (plane polarized light) showing the most relevant petrographic features of the analyzed BM samples. a) phenocrysts/microphenocrysts of alkali feldspar (large crystal at the right), biotite (dark lamella at the left) plagioclase (small dusty individuals with corroded rims at the center and upper center) and clinopyroxene (small light

798 grey crystals at the upper left) set in a glassy groundmass; b) phenocrysts of alkali feldspar (at the
799 left), biotite (light grey lamella at the center) plagioclase (dusty crystal with corroded rims at the
800 upper center), clinopyroxene (grey crystals at the right and lower right) and opaque oxides (black
801 individual at the right) set in a glassy groundmass; c) phenocrysts of alkali feldspar (big crystal at
802 the right) and plagioclase (small dusty individuals with irregular rims at the left and lower left)
803 set in a vescicular glassy matrix; d) phenocrysts of alkali feldspar and plagioclase in a glassy
804 groundmass; e) phenocrysts/microphenocrysts of alkali feldspar (large crystal at the center),
805 plagioclase (tabular crystal at the left) and opaque oxides (black individuals at the lower left) in a
806 glassy groundmass; f) phenocrysts/microphenocrysts of alkali feldspar (large crystal at the left)
807 and plagioclase (tabular crystals at the center and at the right) in a glassy groundmass.

808 Figure 2. Composition of plagioclase and alkali feldspar crystals from the analyzed BM
809 trachytes and trachyphonolites. Small black symbols are for feldspars from the Campi Flegrei
810 district literature (CF; Armienti et al. 1983; Beccaluva et al. 1990; Civetta et al. 1997; de Vita et
811 al. 1999; D'Antonio and Di Girolamo 1994; D'Oriano et al. 2005; Fedele et al. 2006, 2008;
812 Fowler et al. 2007; Melluso et al. 1995, 2012; Orsi et al. 1995; Pappalardo et al. 2002, 2008;
813 Piochi et al. 2005) equilibrated with melts of various compositions. The inset at the upper right
814 shows the composition of the investigated BM whole rock samples (with sample labels in italics)
815 according to R_1R_2 classification (De La Roche et al. 1980).

816 Figure 3. Primitive mantle-normalized [after McDonough and Sun (1995)] trace-element
817 abundances for the analyzed plagioclase (Na- and Ca-rich terms, see text), alkali feldspar and
818 associated glass from the investigated BM trachyte samples AI (a), AN (b) and C (c).

819 Figure 4. Primitive mantle-normalized [after McDonough and Sun (1995)] trace-element
820 abundances for the analyzed plagioclase (Na- and Ca-rich varieties, see text), alkali feldspar and
821 associated glass from the investigated BM trachyphonolite samples B (a), I (b) and R (c).

Figure 5. a) Fe^{2+}+Mn+Mg-Ti-Fe^{3+} classification diagram for the opaque oxides from the analyzed BM trachytes and trachyphonolites. Smaller symbols are literature data for Campi Flegrei trachytes-phonolites (black dots; Armienti et al. 1983, Melluso et al. 1995, 2012, Orsi et al. 1995, Civetta et al. 1997, Pappalardo et al. 2002, 2008, Fedele et al. 2008) and for Ischia latites-trachytes (crosses; Piochi et al. 1999). b) Mg-Al-Fe+Mn classification diagram for the biotite crystals from the analyzed BM trachytes. Smaller symbols are literature data for Campi Flegrei trachytes-phonolites (Armienti et al. 1983, Melluso et al. 1995, 2012, Orsi et al. 1995, Civetta et al. 1997, Fulignati et al. 2004, Fedele et al. 2008, Pappalardo et al. 2008) and for Ischia trachytes-phonolites (Ghiara et al. 1979, Poli et al. 1987, Di Girolamo et al. 1995, Piochi et al. 1999). c) Ca+P vs. Si+REE diagram for the apatite crystals from the analyzed BM trachyphonolites. Smaller symbols are literature data for Campi Flegrei trachytes-phonolites (Fulignati et al. 2004; Fedele et al. 2008; Melluso et al. 2012; authors' unpublished data).

Figure 6. Primitive mantle-normalized [after McDonough and Sun (1995)] trace-element abundances for the analyzed Ti-magnetite and associated glass from the investigated BM trachytes (a and b) and trachyphonolites (c).

Figure 7. Primitive mantle-normalized [after McDonough and Sun (1995)] trace-element abundances for the analyzed biotite (a), apatite (b) and associated glasses from the investigated BM trachytes and trachyphonolites (respectively).

Figure 8. a) Calculated $^{Min/L}D$ values for trace-elements for plagioclase from the investigated BM trachyphonolites. b) $^{Min/L}D$ values for trace-elements calculated applying the model of Bédard (2006) to analyzed plagioclase crystals and coexisting glasses. It is to note that for Eu and Ta the regression equation used is based on the MgO content of the host melt, rather than on plagioclase An content.

845 Figure 9. Calculated $^{Min/L}D$ values for trace-elements for alkali feldspar from the investigated
846 BM trachytes and trachyphonolites.

847 Figure 10. Calculated $^{Min/L}D$ values for trace-elements for Ti-magnetite (a), biotite and apatite
848 (b) from the investigated BM trachytes and trachyphonolites.

Table 1. Average major (EMP, in wt%) and trace element (LA-ICP-HRMS, in ppm) analyses for representative glass from the selected trachytic (T) and trachyphonolitic (Tp) Campi Flegrei BM samples (data from Fedele et al. 2009)

rock	AI (T)		AN (T)		C (T)		B (Tp)		I (Tp)		R (Tp)	
	n = 9, 9		n =7, 7		n = 0, 4		n = 4, 4		n = 4, 6		n = 1, 3	
	Average	S.Dev.	Average	S.Dev.	Average	S.Dev.	Average	S.Dev.	Average	S.Dev.	Average	S.Dev.
SiO_2	60.8	0.44	61.3	0.42	na		60.4	0.33	60.6	0.34	61.8	
TiO_2 (EMP)	0.39	0.07	0.40	0.03	na		0.46	0.03	0.49	0.04	0.43	
Al_2O_3	18.6	0.13	18.9	0.17	na		19.3	0.46	19.5	0.33	17.6	
Cr_2O_3	0.04	0.02	0.04	0.00	na		0.05	0.00	0.00	0.00	0.00	
FeO	3.35	0.26	3.18	0.09	na		3.03	0.08	2.99	0.04	3.33	
MnO	0.15	0.06	0.10	0.02	na		0.26	0.02	0.27	0.08	0.27	
MgO	0.68	0.08	0.64	0.02	na		0.32	0.04	0.43	0.08	0.50	
CaO	2.34	0.23	2.40	0.10	na		1.70	0.05	1.81	0.24	2.42	
Na_2O	3.63	0.61	3.44	0.27	na		6.09	0.17	6.16	0.14	5.23	
K_2O	8.80	0.41	8.95	0.34	na		6.89	0.05	6.81	0.23	7.40	
BaO	0.10	0.05	0.13	0.04	na		bdl	bdl	0.01	0.01	0.00	
F	0.14	0.03	na		na		0.41	bdl	0.43	0.00	na	
SO_3	0.17	0.07	na		na		0.05	bdl	0.07	0.00	na	
Cl	0.20	0.18	0.44	0.06	na		0.78	0.41	0.79	0.42	0.32	
Sum	99.2	0.45	99.8	0.29			99.3	0.84	100.0	0.43	99.3	
Mg#	0.26	0.01	0.26	0.00			0.15	0.01	0.19	0.03	0.20	
P.I.	0.83	0.06	0.81	0.04			0.91	0.04	0.90	0.04	0.94	
Sc	6	0.5	5	0.2	5	0.5	5	0.3	4	0.3	4	0.2
V	43	11.8	45	1.5	57	2.7	14	0.5	15	1.0	16	2.9
TiO_2 (ICP)	0.32	0.03	0.32	0.01	0.34	0.02	0.36	0.02	0.37	0.01	0.43	0.07
Rb	298	42.6	279	16.5	276	21.6	453	28.4	451	16.8	496	23.0
Sr	388	172	360	24	529	73	20	1	25	8	21	3
Y	28	8.9	25	1.3	23	1.4	71	4.3	66	3.9	63	9.3
Zr	296	135	232	9	202	11	853	26	809	53	935	197
Nb	50	24.6	37	1.8	32	1.7	134	5.9	137	10.5	145	32.8
Cs	13	4.9	13	0.6	12	1.2	32	2.3	31	2.1	46	4.3
Ba	418	257	236	14	574	117	13	1	18	4	15	3
La	65	24	55	3	49	5	152	9	148	8	146	12
Ce	120	49	97	7	84	9	270	17	271	23	285	35
Pr	12	4.2	10	0.9	9	1.3	25	1.2	26	1.9	27	3.1
Nd	45	14	40	4	37	4	84	2	92	8	96	9
Sm	7.9	2.1	7.7	0.9	7.2	1.0	14.5	0.5	15.6	1.1	17.8	2.0
Eu	1.84	0.31	2.30	0.23	2.52	0.28	1.32	0.06	1.48	0.15	1.26	0.15

Gd	6.4	1.3	6.1	0.7	5.8	0.5	12.6	1.0	12.7	0.9	13.4	1.7
Tb	0.94	0.15	0.81	0.06	0.76	0.09	1.90	0.16	1.93	0.14	1.76	0.17
Dy	5.7	1.5	4.8	0.6	4.4	0.6	12.6	1.6	12.0	1.0	12.2	1.3
Ho	1.06	0.27	0.92	0.09	0.85	0.06	2.38	0.23	2.28	0.24	2.49	0.34
Er	2.99	0.99	2.53	0.20	2.34	0.14	6.93	0.51	6.94	0.57	7.34	1.34
Tm	0.43	0.14	0.37	0.05	0.37	0.03	1.02	0.02	1.00	0.08	1.12	0.23
Yb	3.1	1.0	2.4	0.2	2.3	0.3	7.0	0.3	6.8	0.5	8.4	2.1
Lu	0.45	0.16	0.36	0.04	0.33	0.07	1.02	0.02	1.04	0.07	1.15	0.13
Hf	6.6	2.8	5.1	0.5	4.9	0.5	16.5	0.7	16.0	1.1	19.4	3.8
Ta	2.4	1.1	1.8	0.1	1.6	0.2	6.3	0.3	6.1	0.3	7.2	1.6
Pb	42.6	5.4	39.9	3.3	38.0	3.8	62.8	3.2	63.2	3.4	84.3	5.1
Th	21.8	10.1	16.8	1.2	15.7	1.7	59.9	1.4	61.1	3.3	67.6	10.1
U	7.6	3.9	5.7	0.4	4.7	0.6	18.5	0.8	19.2	0.9	18.7	2.0

Notes: S.Dev. = standard deviation; n = number of analyses (reported for major and trace elements, separated with a comma); Mg# = molar [Mg/(Mg+Fe+Mn)]. P.I. = molar (Na+K)/Al. bdl = below detection limits; na = not analyzed.

Table 2. Average (Av.) major element concentrations (EMP, in wt%) and calculated structural formulae (apfu, atoms per formula unit, on 8 oxygens and 5 cations) for representative plagioclase (Ca-Pl and Na-Pl) and alkali feldspar (Kfs) crystals from the selected trachytic (T) and trachyphonolitic (Tp) Campi Flegrei BM samples. The full dataset is reported in the Electronic Appendix

rock	AI (Trachyte)				AN (Trachyte)				C (Trachyte)				B (Trachyphonolite)						I (Trachyphonolite)			R (Trachyphonolite)			
phase	Ca-Pl		Kfs		Ca-Pl		Kfs		Ca-Pl		Kfs		Na-Pl		Ca-Pl		Kfs		Na-Pl	Kfs		Na-Pl		Kfs	
	n = 9		n = 4		n = 6		n = 4		n = 6		n = 4		n = 3		n = 5		n = 3			n = 3		n = 6		n = 2	
	Av.	S.Dev.	Av.	S.Dev.	Av.	S.Dev.	Av.	S.Dev.	Av.	S.Dev.	Av.	S.Dev.	Av.	S.Dev.	Av.	S.Dev.	Av.	S.Dev.		Av.	S.Dev.	Av.	S.Dev.	Av.	S.Dev.
SiO_2	46.3	0.75	63.6	0.28	46.5	0.64	64.8	0.57	46.2	0.66	64.1	1.26	60.1	0.57	46.0	0.34	64.5	0.23	60.0	65.0	0.19	61.1	0.62	65.9	0.02
Al_2O_3	33.8	0.48	19.2	0.15	32.9	0.40	18.8	0.25	33.1	0.43	18.9	0.25	24.2	0.11	33.8	0.22	19.3	0.10	24.7	19.4	0.37	23.7	0.28	19.0	0.06
FeO_{tot}	0.66	0.07	0.19	0.06	0.68	0.07	0.20	0.04	0.69	0.06	0.25	0.03	0.42	0.03	0.67	0.03	0.27	0.04	0.37	0.22	0.05	0.41	0.04	0.28	0.02
CaO	16.7	0.59	0.50	0.12	16.2	0.76	0.49	0.07	17.1	0.67	0.44	0.04	5.69	0.28	16.8	0.24	0.68	0.12	6.04	0.68	0.03	6.13	0.42	0.76	0.10
Na_2O	1.53	0.20	1.59	0.16	1.78	0.24	1.54	0.04	1.46	0.19	1.27	0.05	6.97	0.15	1.54	0.10	3.97	0.18	6.95	3.86	0.10	6.88	0.17	4.03	0.09
K_2O	0.32	0.19	13.6	0.24	0.31	0.07	13.7	0.23	0.35	0.09	13.7	0.24	1.87	0.11	0.13	0.03	10.4	0.33	1.83	10.4	0.12	1.80	0.17	10.1	0.28
BaO	0.08	0.02	0.46	0.28	0.07	0.03	0.08	0.02	0.12	0.07	0.62	0.49	0.03	0.01	0.10	0.09	0.05	0.01	bdl	0.04	0.02	0.02	0.00	0.15	0.00
SrO	0.16	0.08	bdl		0.22	0.11	0.21	0.08	0.36	0.10	0.08	0.02	bdl		0.23	0.06	bdl		bdl	bdl		0.08	0.00	0.06	0.00
	99.5	0.36	99.2	0.30	98.7	0.96	99.7	0.40	99.4	0.51	99.3	0.51	99.3	0.45	99.2	0.24	99.2	0.23	99.8	99.5	0.47	100	0.44	100	0.11
Si	2.14	0.03	2.95	0.00	2.17	0.02	3.00	0.02	2.15	0.02	2.99	0.04	2.71	0.01	2.14	0.01	2.95	0.01	2.69	2.97	0.02	2.74	0.03	3.00	0.00
Al	1.84	0.03	1.05	0.00	1.81	0.02	1.02	0.01	1.81	0.03	1.04	0.02	1.28	0.01	1.85	0.01	1.04	0.01	1.30	1.04	0.01	1.25	0.01	1.02	0.00
Fe	0.03	0.00	0.01	0.00	0.03	0.00	0.01	0.00	0.03	0.00	0.01	0.00	0.02	0.00	0.03	0.00	0.01	0.00	0.01	0.01	0.00	0.02	0.00	0.01	0.00
Ca	0.83	0.03	0.03	0.01	0.81	0.04	0.02	0.00	0.85	0.03	0.02	0.00	0.27	0.01	0.83	0.01	0.03	0.01	0.29	0.03	0.00	0.29	0.02	0.04	0.00
Na	0.14	0.02	0.14	0.01	0.16	0.02	0.14	0.00	0.13	0.02	0.11	0.00	0.61	0.01	0.14	0.01	0.35	0.02	0.60	0.34	0.01	0.60	0.01	0.36	0.01
K	0.02	0.01	0.81	0.02	0.02	0.00	0.81	0.01	0.02	0.01	0.82	0.02	0.11	0.01	0.01	0.00	0.61	0.02	0.10	0.60	0.01	0.10	0.01	0.58	0.02
Ba	0.00	0.00	0.01	0.01	0.00	0.00	0.00	0.00	0.00	0.00	0.01	0.01	0.00	0.00	0.00	0.00	0.00	0.00	0.00	0.00	0.00	0.00	0.00	0.00	0.00
Sr	0.00	0.00	0.00	0.00	0.01	0.00	0.00	0.00	0.01	0.00	0.00	0.00	0.00	0.00	0.01	0.00	0.00	0.00	0.00	0.00	0.00	0.00	0.00	0.00	0.00
Total	5.00		5.00		5.00		5.00		5.00		5.00		5.00		5.00		5.00		5.00	5.00		5.00		5.00	
Ab%	14.3	1.87	14.6	1.46	16.8	2.33	14.6	0.06	13.9	1.72	12.1	0.31	61.4	0.96	14.7	0.99	35.5	1.52	60.5	34.9	0.45	60.1	0.98	36.4	0.94
Or%	1.94	1.22	82.9	1.93	1.95	0.38	82.9	0.36	2.21	0.51	85.6	0.40	10.9	0.55	0.89	0.28	61.2	2.08	10.5	61.7	0.58	10.3	1.17	59.8	1.42
An%	83.8	2.80	2.54	0.61	81.3	2.65	2.49	0.36	83.9	2.13	2.30	0.17	27.7	1.51	84.4	1.18	3.33	0.60	29.0	3.41	0.14	29.5	1.65	3.77	0.48

Notes: S.Dev. = standard deviation; n = number of analyses; Ab% = albitite mol%; Or% = orthoclase mol%; An% = anorthite mol%. bdl = below detection limits.

Table 3. Average (Av.) trace element compositions (LA-ICP-HRMS, in ppm) for representative plagioclase (Ca-Pl and Na-Pl) and alkali feldspar (Kfs) crystals from the selected trachytic (T) and trachyphonolitic (Tp) Campi Flegrei BM samples. The full dataset is reported in the Electronic Appendix

rock	AI (Trachyte)			AN (Trachyte)				C (Trachyte)				B (Trachyphonolite)				I (Trachyphonolite)		R (Trachyphonolite)			
phase	Ca-Pl	Kfs		Ca-Pl		Kfs		Ca-Pl		Kfs		Na-Pl	Ca-Pl	Kfs		Na-Pl	Kfs	Na-Pl		Kfs	
		n = 2		n = 2		n = 3		n = 4		n = 2				n = 2				n = 3		n = 2	
		Av.	S.Dev	Av.	S.Dev	Av.	S.Dev	Av.	S.Dev	Av.	S.Dev			Av.	S.Dev			Av.	S.Dev	Av.	S.Dev
Sc	1.7	2.6	0.4	bdl		1.7	0.0	0.8	0.0	0.9	0.0	2.3	1.4	2.5	0.6	1.9	2.1	bdl		bdl	
V	bdl	bdl		bdl		bdl		2.6	1.6	bdl		bdl	bdl	bdl		bdl	bdl	bdl		bdl	
Ti	55.2	208	37.5	57.8	0.18	340	83.3	103	44.5	221	18.5	181	49.0	291	9.19	172	291	178	2.94	289	5.78
Rb	1.2	200	22.6	0.8	0.1	212	12.4	6.9	5.9	170	26.6	11.7	b.d.l.	251	8.2	10.9	269	11.9	1.0	250	11.4
Sr	2420	1140	29.9	2550	93.7	814	360	2780	253	1810	231	303	2220	173	15.3	238	188	199	17.5	183	2.2
Y	0.40	0.04	0.00	0.45	0.00	bdl		0.76	0.48	0.11	0.00	0.19	0.29	bdl		0.28	bdl	0.20	0.04	bdl	
Zr	0.46	b.d.l.		0.38	0.00	bdl		4.09	4.12	bdl		bdl	bdl	bdl		bdl	bdl	bdl		bdl	
Nb	0.18	0.04	0.02	0.08	0.00	bdl		0.82	0.91	bdl		bdl	bdl	bdl		bdl	bdl	0.07	0.03	0.14	0.00
Cs	bdl	0.72	0.03	bdl		0.97	0.03	0.47	0.31	0.77	0.11	bdl	bdl	1.22	0.06	bdl	1.03	bdl		1.19	0.06
Ba	101	2930	1530	122	10.8	664	481	186	19.6	6340	3920	34.4	115	289	18.5	27.5	282	28.1	2.8	310	0.3
La	12.2	2.75	1.44	11.41	0.29	4.63	0.70	10	2.62	1.66	0.34	25.4	7.89	7.94	0.52	29.50	9.12	27.8	1.69	7.98	0.20
Ce	16.7	1.85	1.05	15.80	0.14	2.94	0.48	14	3.40	1.06	0.28	26.1	10.8	4.94	0.48	31.73	6.31	29.1	1.97	5.53	0.15
Pr	1.30	0.10	0.04	1.31	0.11	0.18	0.04	1.36	0.33	0.08	0.02	1.61	0.98	0.28	0.03	2.19	0.33	1.89	0.04	0.28	0.01
Nd	3.99	0.16	0.07	4.55	0.18	0.31	0.11	4.80	1.21	0.13	0.05	4.30	3.06	0.38	0.02	5.86	0.65	5.58	0.44	0.46	0.02
Sm	0.50	0.05	0.01	0.48	0.11	bdl		0.61	0.14	0.03	0.00	0.33	0.43	0.04	0.00	0.44	0.08	0.30	0.02	bdl	
Eu	1.37	1.37	0.32	1.64	0.12	2.39	0.22	1.53	0.02	1.40	0.21	1.50	1.14	1.65	0.17	1.81	1.91	1.74	0.17	1.73	0.07
Gd	0.37	bdl		0.35	0.00	bdl		0.50	0.10	bdl		0.35	0.21	bdl		bdl	bdl	bdl		bdl	
Tb	bdl	bdl		0.02	0.00	bdl		0.05	0.02	bdl		bdl	bdl	bdl		bdl	bdl	bdl		bdl	
Dy	bdl	bdl		bdl		bdl		0.23	0.12	bdl		bdl	0.20	bdl		0.17	bdl	bdl		bdl	
Ho	bdl	bdl		bdl		bdl		0.04	0.02	bdl		bdl	0.01	bdl		bdl	bdl	bdl		bdl	
Er	bdl	bdl		bdl		bdl		0.13	0.00	bdl		bdl	bdl	bdl		0.06	bdl	bdl		bdl	
Tm	bdl	bdl		bdl		bdl		bdl		bdl		bdl	bdl	bdl		bdl	bdl	bdl		bdl	
Yb	bdl	bdl		bdl		bdl		bdl		bdl		0.01	bdl	bdl		bdl	bdl	bdl		bdl	
Lu	bdl	bdl		bdl		bdl		bdl		bdl		bdl	bdl	bdl		bdl	bdl	bdl		bdl	
Hf	bdl	bdl		bdl		bdl		0.28	0.00	0.03	0.00	bdl	bdl	bdl		bdl	bdl	bdl		bdl	
Ta	bdl	0.03		bdl		bdl		0.12	0.00	bdl		bdl	bdl	bdl		bdl	bdl	bdl		bdl	
Pb	5.84	16.3	2.34	5.89	0.14	22.7	0.96	5.97	0.76	14.4	2.46	15.1	5.19	26.2	0.03	15.3	28.2	17.2	0.78	29.0	0.52
Th	0.06	bdl		0.03	0.00	bdl		0.35	0.37	bdl		bdl	bdl	bdl		0.01	bdl	bdl		bdl	
U	0.01	bdl		0.01	0.00	bdl		0.12	0.13	bdl		0.01	bdl	bdl		bdl	bdl	bdl		0.01	0.00

Notes: S.Dev. = standard deviation; n = number of analyses; bdl = below detection limits.

Table 4. Major element concentrations (EMP, in wt%) and calculated structural formulae (in apfu, atoms per formula unit) for representative Ti-magnetite (Mt, 3 cations and 4 oxygens basis), biotite and (Bt and Ap, 16 cations and 24 oxygens) from the selected trachytic (T) and trachyphonolitic (Tp) Campi Flegrei BM samples

rock	AI (T)	AN (T)	I (Tp)		AI (T)			I (Tp)
sample	AI-2-MAGN18-3	AN-2-MAGN 10-2	I-5-MAGN22-9		AI-1-BIOT14-10	AI-3-BIOT36-12		I-5-APAT22-3
phase	Mt	Mt	Mt		Bt	Bt		Ap
TiO_2	5.78	5.68	9.50	SiO_2	36.4	36.3	SiO_2	1.03
Al_2O_3	4.43	3.88	1.93	TiO_2	4.83	4.87	FeO_{tot}	0.28
FeO_{tot}	79.4	80.3	80.3	Al_2O_3	14.5	14.9	CaO	52.0
MnO	0.56	0.58	1.96	Cr_2O_3	0.01	0.00	F	3.83
MgO	2.74	2.42	1.49	FeO_{tot}	13.9	14.2	P_2O_5	42.5
	92.9	92.8	95.2	MnO	0.17	0.23		99.7
				MgO	15.9	15.7	O=F	1.61
Fe_2O_3	52.8	53.5	49.3	CaO	0.01	0.02	Tot	98.1
FeO	31.8	32.1	36.0	K_2O	9.22	9.29		
Usp%	17.4	17.0	26.6	Na_2O	0.31	0.25	T site (6 cations)	
				BaO	0.29	0.62	Si	0.17
Si	0.00	0.00	0.00	Cl	0.08	bdl	P	5.83
Ti	0.16	0.16	0.27	SrO	bdl	0.17	M1+M2 sites (10 cations)	
Al	0.19	0.17	0.08		95.7	96.5	Ca	9.96
Fe^{+3}	1.48	1.51	1.38				Fe	0.04
Fe^{+2}	0.99	1.01	1.12	Mg#	0.67	0.66		
Mn	0.02	0.02	0.06					
Mg	0.15	0.14	0.08	Si	5.42	5.38		
				Ti	0.54	0.54		
				Al^{IV}	2.04	2.08		
				Al^{VI}	0.52	0.54		
				Mg	3.52	3.48		
				Fe	1.73	1.76		
				Mn	0.02	0.03		
				$\square_{M1}$	0.20	0.20		
				K	1.75	1.76		
				Na	0.09	0.07		
				$\square_A$	0.16	0.17		

Notes: FeO and Fe_2O_3 in Ti-magnetite calculated following Carmichael (1967). Ulvöspinel mol% (Usp%) calculated according to Stormer (1983). $\square_A$ and $\square_{M1}$ for the biotite are the vacancies in the dodecahedral site A and in the octahedral site M1. St.Dev. = standard deviation; n = number of analyses; Mg# = molar Mg/(Fetot+Mg+Mn). bdl = below detection limits.

Table 5. Trace element compositions (LA-ICP-HRMS, in ppm) for representative Ti-magnetite (Mt), biotite (Bt) and apatite (Ap) from the selected trachytic (T) and trachyphonolitic (Tp) Campi Flegrei BM samples

rock		AI (T)		AN (T)	I (Tp)	
sample	AI-2-MAGN18-3	AI-1-BIOT14-10	AI-3-BIOT36-12	AN-2-MAGN 10-2	I-5-MAGN22-9	I-5-APAT22-3
phase	Mt	Bt	Bt	Mt	Mt	Ap
Sc	9.3	12.2	13.0	8.4	4.3	bdl
V	2400	426	486	1960	823	29.8
Cr	113	15.4	13.9	157	50.8	bdl
Rb	bdl	307	294	bdl	bdl	bdl
Sr	bdl	68.8	95.3	bdl	bdl	81.0
Y	0.11	0.07	0.20	0.31	0.25	1490
Zr	21.9	21.5	22.1	23.9	69.3	bdl
Nb	8.5	47.6	40.9	10.3	50.6	bdl
Cs	bdl	3.22	3.29	bdl	bdl	bdl
Ba	bdl	2900	5270	bdl	bdl	8.02
La	bdl	bdl	bdl	bdl	bdl	3630
Ce	bdl	bdl	bdl	bdl	bdl	7330
Pr	bdl	bdl	bdl	bdl	bdl	879
Nd	bdl	bdl	bdl	bdl	bdl	3570
Sm	bdl	bdl	bdl	bdl	bdl	518
Eu	bdl	bdl	bdl	bdl	bdl	43.4
Gd	bdl	bdl	bdl	bdl	bdl	412
Tb	bdl	bdl	bdl	bdl	bdl	47.7
Dy	bdl	bdl	bdl	bdl	bdl	273
Ho	bdl	bdl	bdl	bdl	bdl	48.6
Er	bdl	bdl	bdl	bdl	bdl	117
Tm	bdl	bdl	bdl	bdl	bdl	13.1
Yb	bdl	bdl	bdl	bdl	0.06	65.2
Lu	bdl	bdl	bdl	bdl	bdl	8.08
Hf	0.56	0.57	0.62	0.66	2.10	bdl
Ta	0.44	1.85	1.68	0.46	2.21	bdl
Pb	bdl	1.85	2.39	bdl	0.59	13.7
Th	bdl	bdl	0.03	0.05	0.01	110
U	0.01	0.03	0.03	0.02	0.04	14.4

Notes: St.Dev. = standard deviation; n = number of analyses; bdl = below detection limits.

Table 6. Calculated $^{Pl/L}D$ values for the selected BM trachyphonolites (Pl/Tp)

	Pl/Tp			Feld/T	Feld/Tp	Pl/T	Pl/Tp	Pl/Ph
sample	B	I	R	Vil1988		Pap2008		Wo1983
Rb	0.03	0.02	0.02	0.7-0.97	0.52			0.018-0.052
Ba	2.6	1.5	1.8	1.13-16.6	9.50	0.05	0.90	1.725-7.33
Th	0.0001	0.0002		0.01-0.03	0.01			0.001-0.008
U	0.0007			0.01-0.03	0.01			
La	0.17	0.20	0.19	0.08-0.10	0.09	0.40	0.18	0.251-0.343
Ce	0.10	0.12	0.10			0.20	0.10	0.129-0.212
Pb	0.24	0.24	0.20					
Sr	15	9.5	9.5	2-6.6		1.40	7.80	11.66-49.8
Pr	0.065	0.086	0.069					
Nd	0.051	0.064	0.058			0.15	0.05	0.055-0.168
Sm	0.023	0.028	0.017			0.08	0.02	0.080-0.130
Eu	1.1	1.2	1.4	0.85-1.06	1.17	0.90	0.80	0.991-2.178
Gd	0.03							
Ti	0.08	0.08	0.07					
Dy		0.01						
Y	0.003	0.004	0.003					
Er		0.01						
Yb	0.001							0.003-0.009
Sc	0.48	0.42		0.03-0.07	0.26			0.015-0.055

	Pl/NaT				Pl/Rhy		Pl/hsR	
	Nag1973	Lem1987	D'O1998	N&C1985	B&D1988	I&L1996	E&G1994	S&G1997
Rb		0.06	0.074	0.06-0.19	0.30	0.07-0.76	0.011-0.029	0.13-0.34
Ba	0.265-3.40		0.78	0.56-3.3	0.48	1.07-18.38	1.00-1.8	6.95-19.55
Th		0.01	0.010	0.03-0.08	0.01			0.03
U		0.01	0.018	0.05-0.13				
La		0.05	0.21	0.30-0.45	0.30			0.070-0.17
Ce	0.0115-0.223		0.13	0.21-0.34	0.22			0.032-0.104
Pb			0.27	0.42-2.2			0.35-0.97	
Sr	0.94-3.18		4.2	6.8-33	4.40	7.96-23.05	4.04-12.2	10.5-13.1
Pr	0.0078-0.219		0.100					
Nd			0.080	0.14-0.29	0.19			
Sm			0.046	0.11-0.23	0.12			0.008-0.019
Eu	1.52-2.35	0.27	0.65	3.8-7.9	2.00			3.75-5.62
Gd								
Ti								
Dy	0.043-0.220		0.021	0.07-0.18				
Y			0.021	0.04-0.21			0.022-0.084	
Er	0.037-0.219		0.017					
Yb	0.037-0.227		0.021	0.06-0.13	0.10			0.012-0.026
Sc		0.01		0.02-0.06	0.01			

Notes: Also shown are literature data for Campi Flegrei trachytes (Pl/T) and trachyphonolites (from Vil1988 = Villemant 1988 and Pap2008 = Pappalardo et al. 2008), for phonolites (Pl/Ph; from Wo1983 = Wörner et al. 1983), sodic trachytes (Pl/NaT; from Nag1973 = Nagasawa 1973, Lem1987 = Lemarchand et al. 1987 and D'O1998 = D'Orazio et al. 1998), rhyolites (Pl/Rhy; from N&C1985 = Nash and Crecraft 1985, B&D1988 = Bacon and Druitt 1988 and I&L1996 = Icenhower and London 1996) and high-silica rhyolites (Pl/hsR; from E&G1994 = Ewart and Griffin 1994 and S&G1997 = Streck and Grunder 1997). Data from Villemant (1988) refer to feldspar/liquid equilibria (Feld/T and Feld/Tp), not taking into account whether plagioclase or alkali feldspar.

Table 7. Calculated $^{Kfs/L}D$ values for the selected BM trachytes (Kfs/T) and trachyphonolites (Kfs/Tp)

	Kfs/T		Kfs/Tp			Feld/T	Feld/Tp	Kfs/T	Kfs/Tp	Kfs/T	Kfs/Ph
sample	AI	AN	AN	B	I	R	Vil1988		Pap2008		Wh2003	Wo1983
Cs	0.07	0.08	0.07	0.04	0.03	0.03	0.08-0.12	0.04			0.04	
Rb	0.81	0.78	0.70	0.55	0.60	0.50	0.7-0.97	0.52			0.24-0.37	0.55-1.25
Ba	2.8	2.5	5.4	21	16	20	1.13-16.6	9.50	0.3-13	7.70	1.11-12.74	0.36-9.36
U				0.0001		0.0004	0.01-0.03	0.01				
Nb	0.002					0.001					0.03	
Ta							0.01-0.03					0.008-0.009
La	0.08	0.10	0.07	0.05	0.06	0.05	0.08-0.10	0.09	0.13	0.05	0.03-0.06	0.058-0.132
Ce	0.03	0.04	0.03	0.02	0.02	0.02			0.04	0.02	0.02-0.06	0.009-0.050
Pb	0.47	0.57	0.54	0.42	0.45	0.34						
Sr	2.5	2.8	3.1	8.8	7.5	8.7	2-6.6		2.00	7.10	0.45-4.81	3.21-8.17
Pr	0.014	0.022	0.016	0.011	0.013	0.010					0.01-0.04	
Nd	0.006	0.012	0.006	0.004	0.007	0.005			0.01	0.005	0.01-0.04	0.090-0.130
Sm	0.009			0.003	0.005						0.01-0.04	0.004-0.015
Eu	0.87	1.2	0.93	1.2	1.3	1.4	0.85-1.06	1.17	0.90	0.80	2.04-2.10	0.46-0.991
Ti	0.13	0.24	0.13	0.13	0.13	0.11						
Y											0.01-0.06	
Sc	0.54	0.35		0.53	0.47		0.03-0.07	0.26				0.016-0.20

	Kfs/NaT	Kfs/Pnt	Kfs/Pnt	Kfs/Com		Kfs/Rhy		Kfs/hsR	
	M&S1990		Wh2003		L&P1981	M&H1983	N&C1985	S&G1990	E&G1994
Cs	0.0075-0.013	0.0004-0.0036	0.04-0.24	0.04-0.30	0.024	0.009-0.61	0.11-0.37	0.002-0.61	
Rb	0.11-0.26	0.25	0.21-0.37	0.22-0.51	0.4	0.31-0.74	1.2-2.4	0.28-0.74	0.11-0.72
Ba	5.2-5.9	1.2-1.6	1.87-12.22	0.66-10.35	22	1.00-6.7	4.9-24	1.0-44	2.7-20.9
U						0.008-0.037	0.04-0.07	0.002-0.037	
Nb			0.01-0.04	0.01-0.14					0.039-0.16
Ta					0.015	0.0045-0.029	0.001-0.02	0.0007-0.029	
La	0.042-0.0707	0.0007-0.0018	0.01-0.09	0.05-0.16	0.129	0.037-0.111	0.07-0.10	0.026-0.15	
Ce	0.0024-0.0349	0.0005-0.0018	0.01-0.06	0.05-0.14	0.065	0.031-0.095	0.02-0.06	0.017-0.095	
Pb			1.00	0.22			0.99-4.1		0.10-1.4
Sr	3.6-10	0.9-1.24	0.40-4.06	0.53-2.79			4.5-7.3	2-6	2.11-22.1
Pr			0.01-0.07	0.05-0.14					
Nd			0.02-0.07	0.05-0.12	0.054	0.013-0.093	0.03-0.04	0.009-0.093	
Sm	0.0018-0.0086	0.0004-0.0018	0.02-0.10	0.05-0.09	0.026	0.014-0.0458	0.03-0.04	0.0024-0.046	
Eu	0.439-2.50	0.0238-0.049	0.05-0.24	0.60-2.16	9.06	2-3.5	3.3-6.5	1.6-9.6	
Ti									
Y									0.015-0.067
Sc	0.0051-0.0063	0.0067-0.0094			0.029	0.024-0.059	0.01-0.04		

Notes: Also shown are literature data for Campi Flegrei trachytes and trachyphonolites, for trachytes, phonolites (Kfs/Ph), sodic trachytes (Kfs/NaT), pantellerites (Kfs/Pnt), comendites (Kfs/Com), rhyolites (Pl/Rhy) and high-silica rhyolites (Pl/hsR). L&P1981 = Leeman and Phelps 1981. M&H1983 = Mahoood and Hildreth 1983. M&S1990 = Mahood and Stimac 1990. S&G1990 = Stix and Gorton 1990. Wh2003 = White et al. 2003. Other abbreviations as in Table 6 caption. Data from Villemant (1988) refer to feldspar/liquid equilibria (Feld/T and Feld/Tp), not taking into account whether plagioclase or alkali feldspar.

Table 8. Calculated $^{Mt/L}D$ values for the selected BM trachytes (Mt/T) and trachyphonolites (Mt/Tp)

	Mt/T		Mt/Tp	Mt/T	Mt/Tp	Mt/Ph	Mt/NaT		Mt/Rhy		Mt/hsR	
sample	AI	AN	I	Vil1988		Wo1983	Lem1987	M&S1990	N&C1985	B&D1988	M&H1983	E&G1994
Th		0.0033	0.0002	0.17-0.21	0.18	0.053-0.805	0.06	0.002-0.02	0.09-0.32	0.01	1.63-13.1	
U	0.0016	0.0031	0.0023	0.11-0.14	0.12	0.725	0.09		0.21-0.83		0.74	
Nb	0.23	0.27	0.37									
Ta	0.24	0.26	0.37	0.47-0.55	0.42	0.164-0.90	1.13	1.36-2.35	2.3-4.5	1.2	0.74-2.73	
Pb			0.009									
Zr	0.097	0.10	0.086	0.21-0.25			0.62	0.17-0.29		0.24		0.37
Hf	0.11	0.13	0.13	0.27-0.31	0.20	0.032-0.13	0.51	0.10-0.29	0.95-2.9	0.24		
Ti	19	18	25									
Y	0.005	0.012	0.004									3.21
Yb			0.01			0.35-0.42		0.01-0.06	1.0-2.2	0.44	1.30	
Sc	1.7	1.7	0.96	3.8-7.95	9.70	2.85-5.38	10.42	1.88-3.33	1.5-15.6	5.0	8.9-12.4	
V	49	44	55									

Notes: Also shown are literature data for Campi Flegrei trachytes and trachyphonolites, for phonolites (Mt/Ph), sodic trachytes (Mt/NaT), rhyolites (Mt/Rhy) and high-silica rhyolites (Mt/hsR). N&C1985 = Nash and Crecraft 1985. Other abbreviations as in Tables 6 and 7 captions.

Table 9. Calculated $^{Bt/L}D$ values for the selected BM trachytes (Bt/T)

	Bt/T		Bt/T	Bt/Ph	Bt/Rhy	Bt/hsR	
sample	AI	AI	Vill988	Wo1983	N&C1985	M&H1983	E&G1994
Cs	0.32	0.32	0.56-0.79		1.2-4.4	1.2-3.1	
Rb	1.1	1.1	1.35-1.58	1.1-2.321	2.3-4.1	3.0-5.3	9.70
Ba	5.7	10	1.04-21.5	10.1-11.2	5.6-36	3.7-7.0	
Th		0.002	0.09-0.11	0.08	0.27-2.0	0.511-1.74	
U	0.005	0.005	0.08	0.198	0.46-1.2	0.131-0.19	
Nb	1.3	1.1			4.0-9.5		9.10
Ta	1.0	0.93	0.74-1.02	0.26-0.325	1.2-1.9	1.31-1.36	
Pb	0.046	0.060			0.1-1.6		2.10
Sr	0.15	0.20	0.20-0.78		0.29-0.53		7.20
Zr	0.096	0.098	0.13-0.28		0.79-1.8		0.47
Hf	0.11	0.12	0.13-0.15	0.047-0.10	0.44-0.84	0.47-0.68	
Ti	14	14					
Y	0.003	0.008			1.0-1.4		2.40
Sc	2.2	2.3	2.81-5.56	23.20-26.8	4.9-20	13.1-18.1	
V	8.8	10.0					

Notes: $^{Bt/L}D_{Ti}$ was calculated on the basis of EMP data. Also shown are literature data for $^{Bt/L}D$ calculated for Campi Flegrei trachytes, for phonolites (Bt/Ph), rhyolites (Bt/Rhy) and high-silica rhyolites (Bt/hsR). Abbreviations for data sources as in Tables 6, 7 and 8 captions.

Table 10. Calculated $^{Ap/L}D$ values for the selected BM trachyphonolites (Ap/Tp)

	Ap/Tp	Ap/Ph	Ap/NaT	Ap/Pnt	Ap/G	
sample	I	Wo1983	M&S1990		Nag1970	W&G1981
Ba	0.45		0.45			
Th	1.8	1.2	1.6			
U	0.75		2.6			
La	25	14.4	13-39	36-38		8.0-11.9
Ce	27	24.3	28-46	40-43	29.6	
Pb	0.22					
Sr	3.3					2.1-2.4
Pr	34					
Nd	39	54.3	23-38	35-38	57.1	
Sm	33	95.2	38		84.8	18.5-38.4
Eu	29	102	30.2		9.22	
Gd	32					
Tb	25	41.4	30			
Ti	0.05					
Dy	23				246	15.9-30.7
Ho	21					
Y	23		20-21	11-12		
Er	17				275	
Tm	13					
Yb	9.6	8.81	10		232	
Lu	7.8	3.69	7.2		199	7.5-20.4
V	2.0					

Notes: Also shown are literature data for $^{Ap/L}D$ calculated for phonolites (Ap/Ph), granites (Ap/G), sodic trachytes (Ap/NaT) and pantellerites (Ap/Pnt). Nag1970 = Nagasawa 1970. W&G1981 = Watson and Green 1981. Other abbreviations as in Tables 6, 7 and 8 captions.

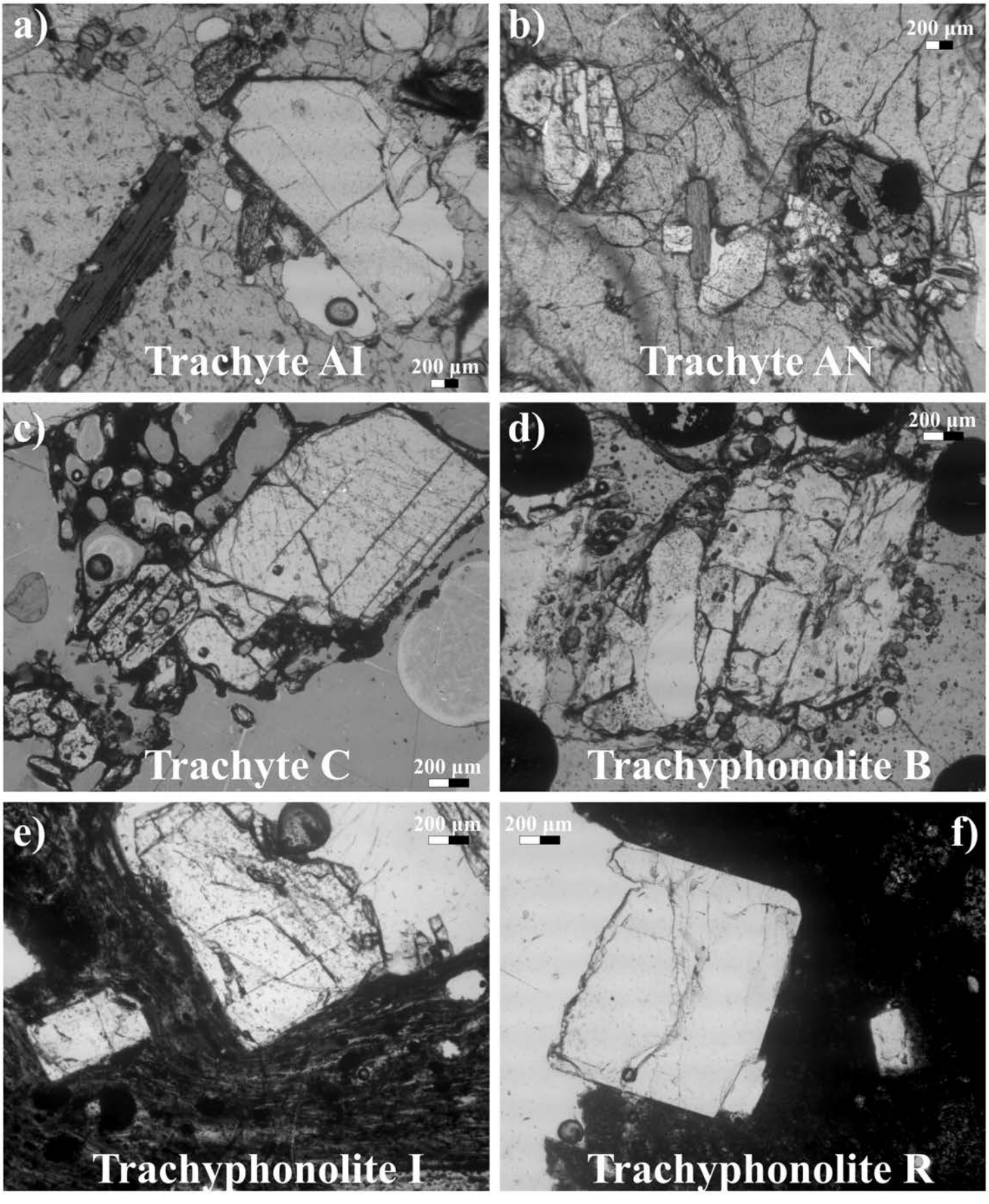
a)
Trachyte AI
200 µm
b)
200 µm
Trachyte AN
c)
Trachyte C
200 µm
d)
200 µm
Trachyphonolite B
e)
200 µm
Trachyphonolite I
200 µm
f)
Trachyphonolite R

Fig.1

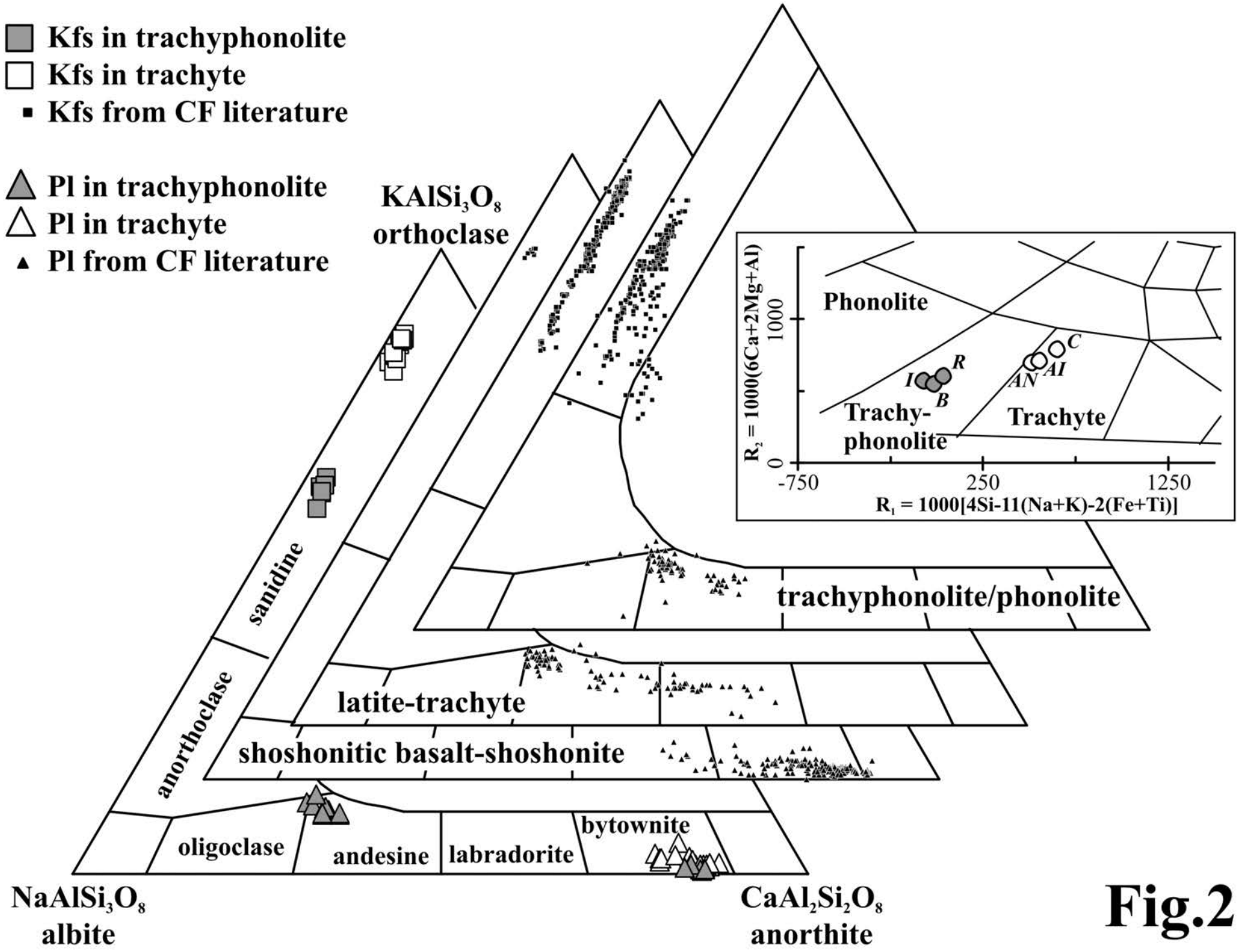
Kfs in trachyphonolite
Kfs in trachyte
Kfs from CF literature
Pl in trachyphonolite
Pl in trachyte
Pl from CF literature
KAlSi3O8
orthoclase
sanidine
anorthoclase
NaAlSi3O8
albite
CaAl2Si2O8
anorthite
trachyphonolite/phonolite
latite-trachyte
shoshonitic basalt-shoshonite
oligoclase
andesine
labradorite
bytownite
Phonolite
Trachy-
phonolite
Trachyte
R
I
B
C
AI
AN
R2 = 1000(6Ca+2Mg+Al)
1000
0
-750
250
1250
R1 = 1000[4Si-11(Na+K)-2(Fe+Ti)]

Fig.2

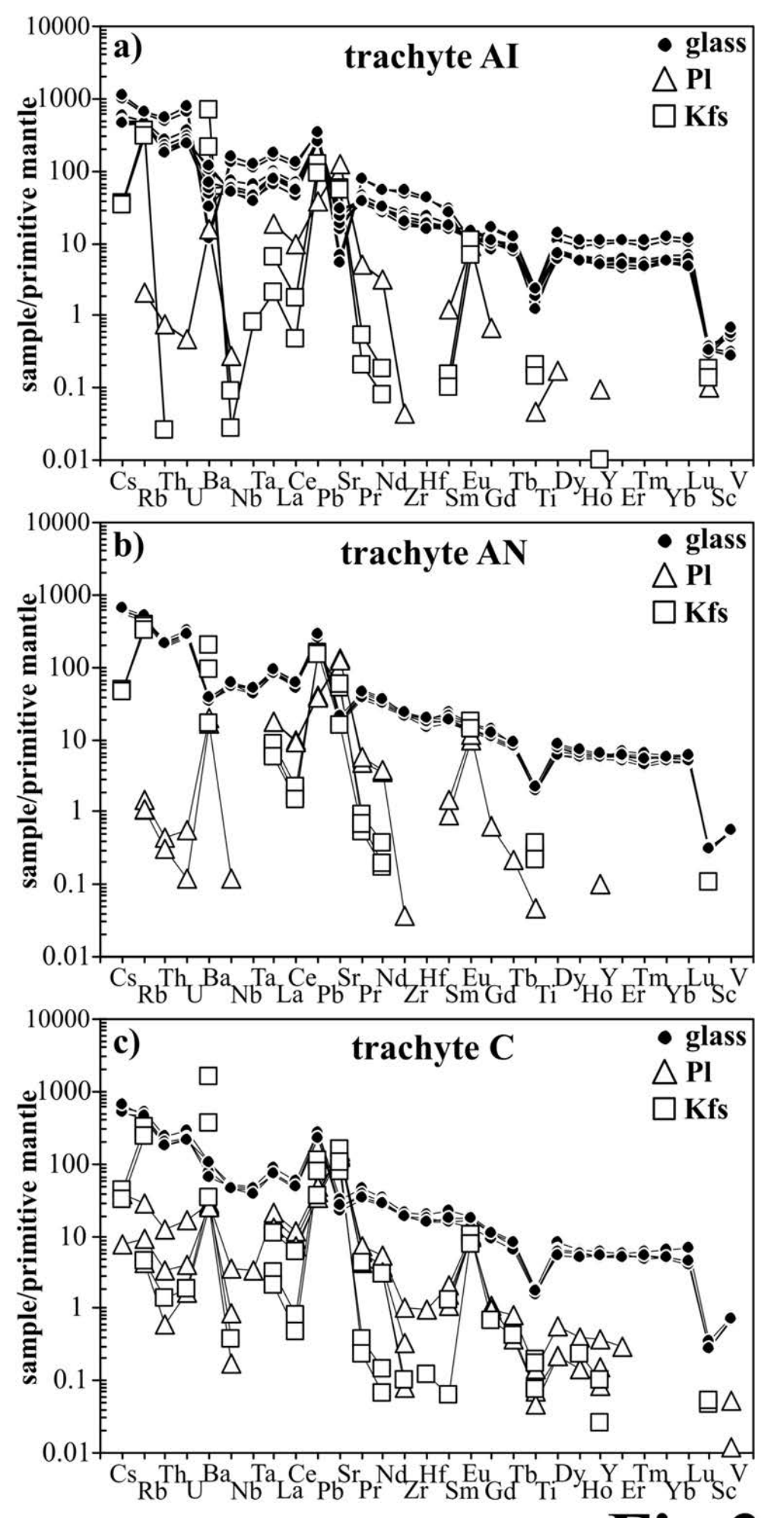
a)
trachyte AI
glass
Pl
Kfs
sample/primitive mantle
10000
1000
100
10
1
0.1
0.01
Cs Rb Th U Ba Nb Ta La Ce Pb Sr Pr Nd Zr Hf Sm Eu Gd Tb Ti Dy Ho Y Er Tm Yb Lu Sc V
b)
trachyte AN
glass
Pl
Kfs
sample/primitive mantle
10000
1000
100
10
1
0.1
0.01
Cs Rb Th U Ba Nb Ta La Ce Pb Sr Pr Nd Zr Hf Sm Eu Gd Tb Ti Dy Ho Y Er Tm Yb Lu Sc V
c)
trachyte C
glass
Pl
Kfs
sample/primitive mantle
10000
1000
100
10
1
0.1
0.01
Cs Rb Th U Ba Nb Ta La Ce Pb Sr Pr Nd Zr Hf Sm Eu Gd Tb Ti Dy Ho Y Er Tm Yb Lu Sc V

Fig.3

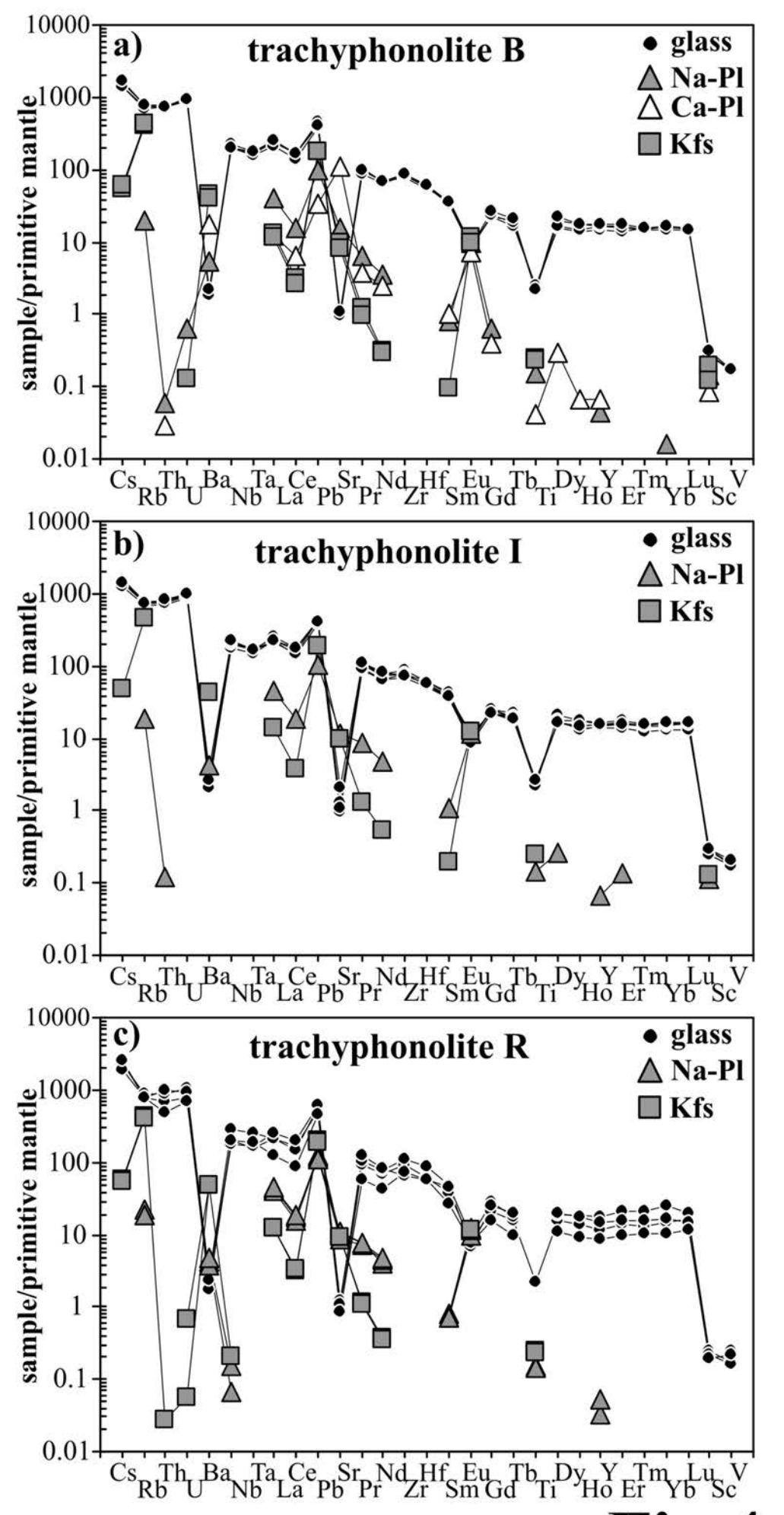
a)
trachyphonolite B
glass
Na-Pl
Ca-Pl
Kfs
sample/primitive mantle
10000
1000
100
10
1
0.1
0.01
Cs Rb Th U Ba Nb Ta La Ce Pb Sr Pr Nd Zr Hf Sm Eu Gd Tb Ti Dy Ho Y Er Tm Yb Lu Sc V
b)
trachyphonolite I
glass
Na-Pl
Kfs
sample/primitive mantle
10000
1000
100
10
1
0.1
0.01
Cs Rb Th U Ba Nb Ta La Ce Pb Sr Pr Nd Zr Hf Sm Eu Gd Tb Ti Dy Ho Y Er Tm Yb Lu Sc V
c)
trachyphonolite R
glass
Na-Pl
Kfs
sample/primitive mantle
10000
1000
100
10
1
0.1
0.01
Cs Rb Th U Ba Nb Ta La Ce Pb Sr Pr Nd Zr Hf Sm Eu Gd Tb Ti Dy Ho Y Er Tm Yb Lu Sc V

Fig.4

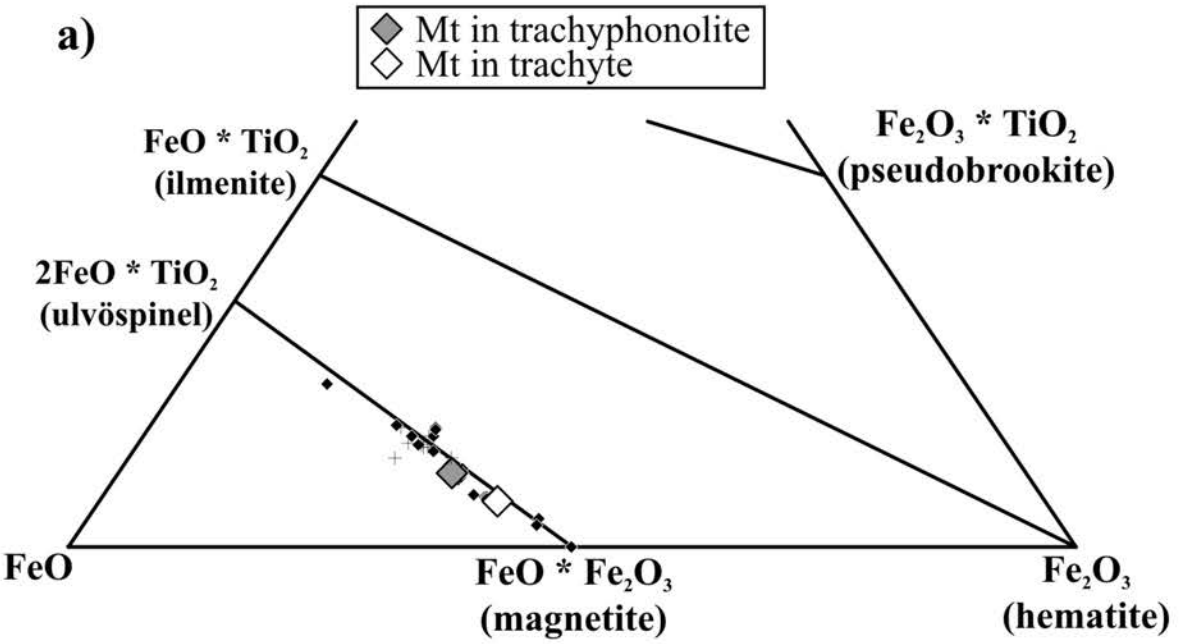
a)
Mt in trachyphonolite
Mt in trachyte
FeO * TiO2
(ilmenite)
Fe2O3 * TiO2
(pseudobrookite)
2FeO * TiO2
(ulvöspinel)
FeO
FeO * Fe2O3
(magnetite)
Fe2O3
(hematite)

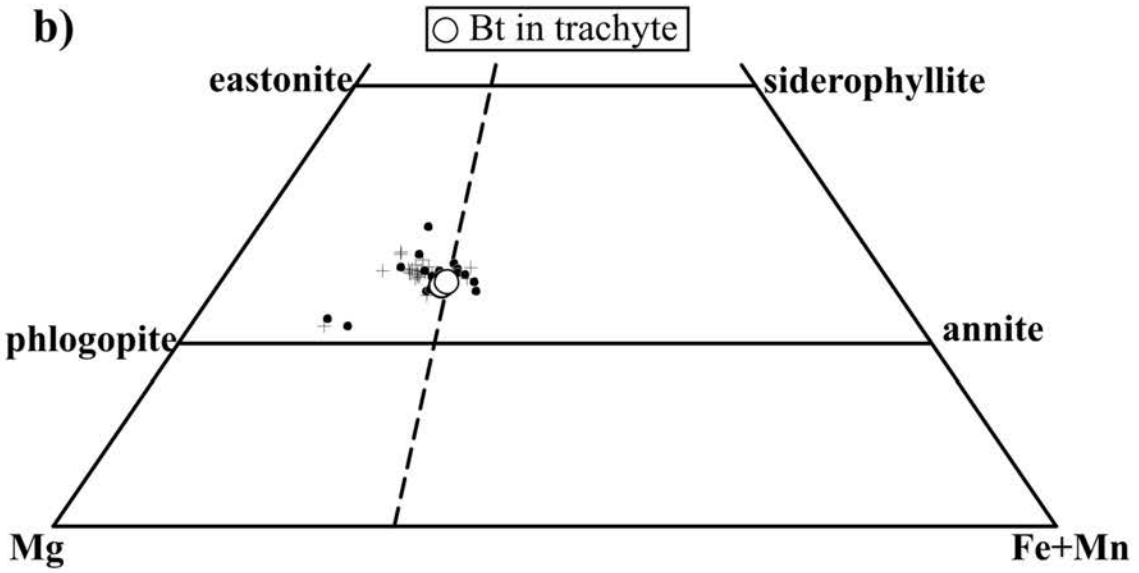
b)
Bt in trachyte
eastonite
siderophyllite
phlogopite
annite
Mg
Fe+Mn

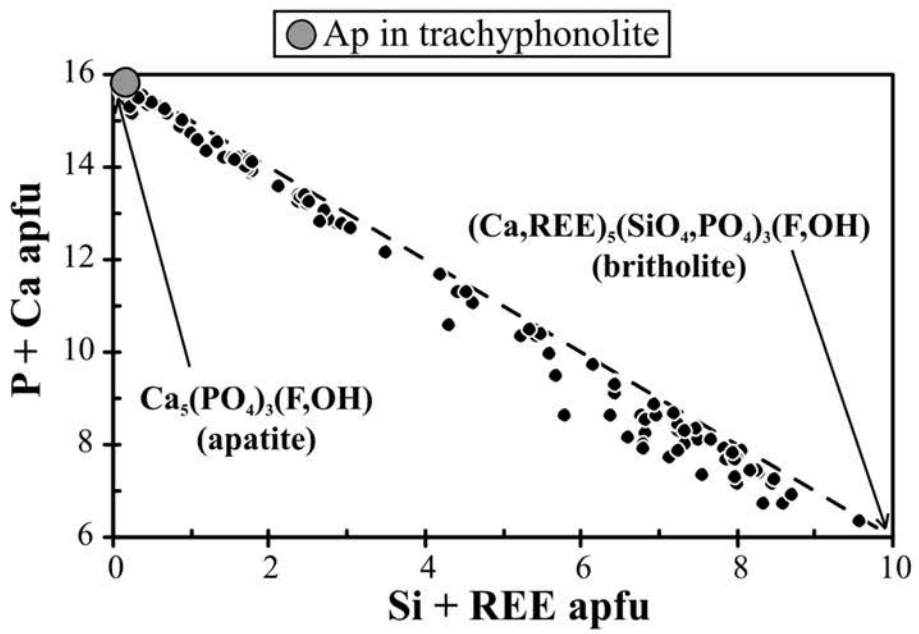
c)
Ap in trachyphonolite
P + Ca apfu
Si + REE apfu
(Ca,REE)5(SiO4,PO4)3(F,OH)
(britholite)
Ca5(PO4)3(F,OH)
(apatite)
16
14
12
10
8
6
0
2
4
6
8
10

Fig.5

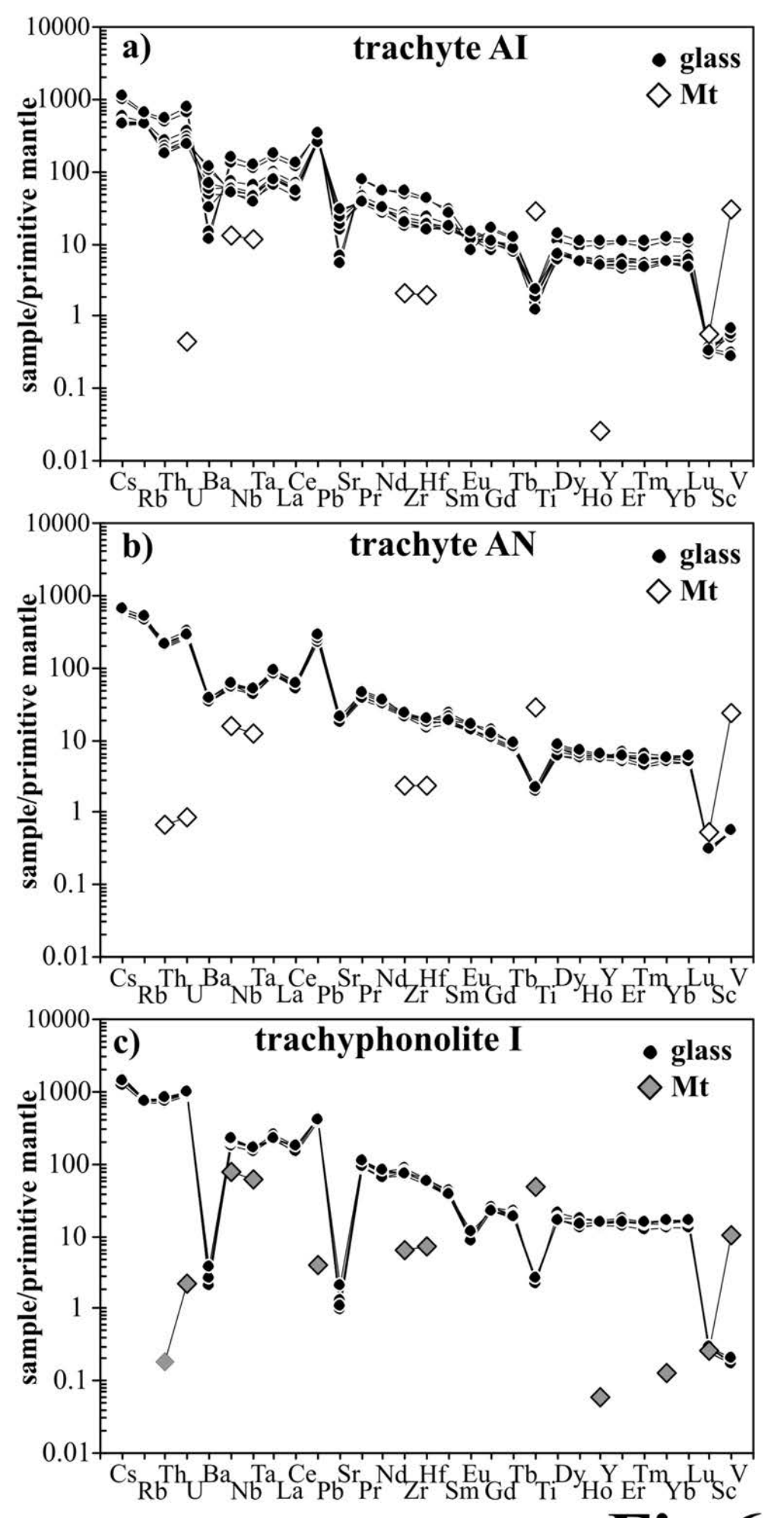
a)
trachyte AI
glass
Mt
sample/primitive mantle
10000
1000
100
10
1
0.1
0.01
Cs Rb Th U Ba Nb Ta La Ce Pb Sr Pr Nd Zr Hf Sm Eu Gd Tb Ti Dy Ho Y Er Tm Yb Lu Sc V
b)
trachyte AN
glass
Mt
sample/primitive mantle
Cs Rb Th U Ba Nb Ta La Ce Pb Sr Pr Nd Zr Hf Sm Eu Gd Tb Ti Dy Ho Y Er Tm Yb Lu Sc V
c)
trachyphonolite I
glass
Mt
sample/primitive mantle
Cs Rb Th U Ba Nb Ta La Ce Pb Sr Pr Nd Zr Hf Sm Eu Gd Tb Ti Dy Ho Y Er Tm Yb Lu Sc V

Fig.6

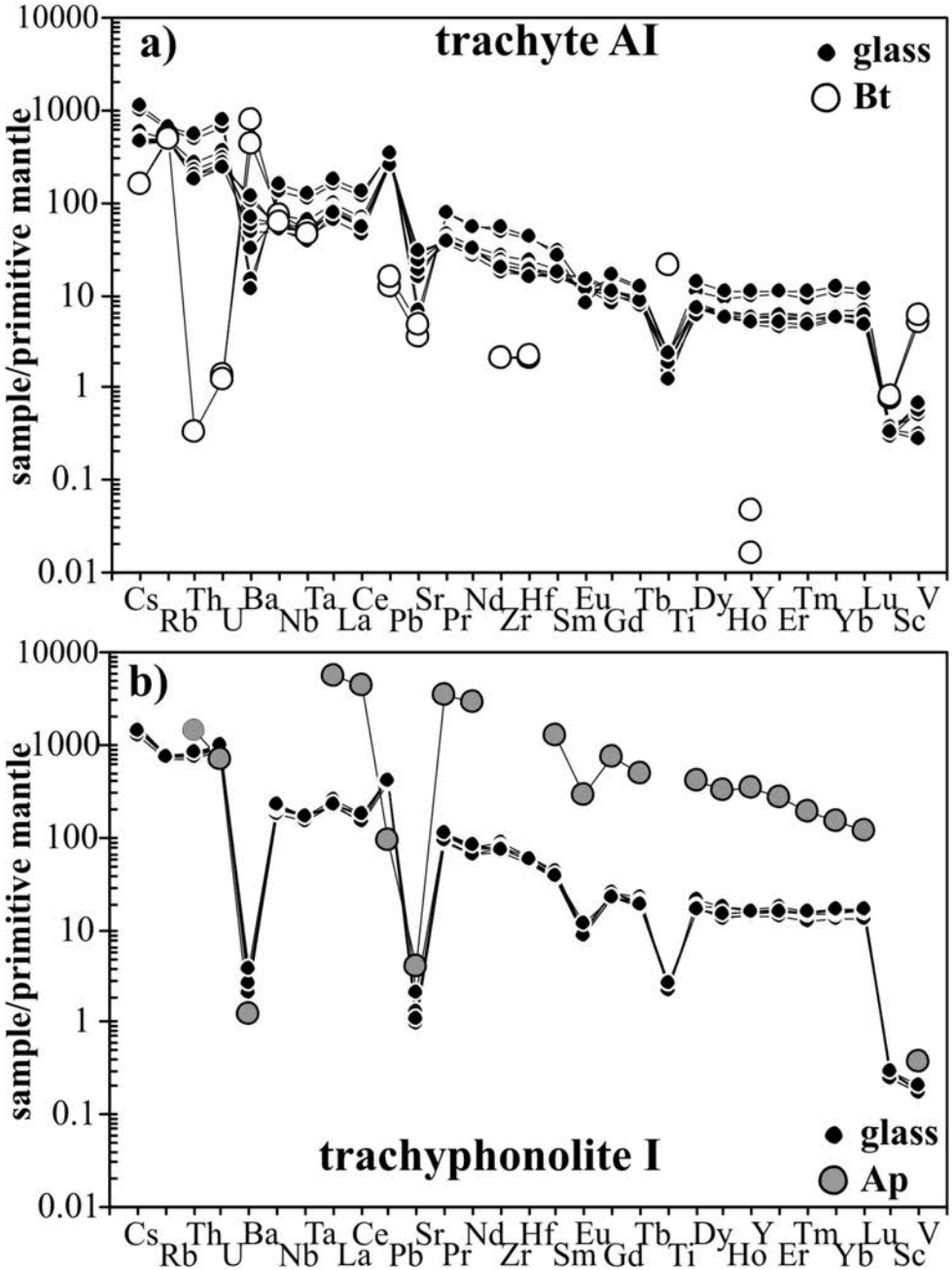
a)
trachyte AI
glass
Bt
sample/primitive mantle
10000
1000
100
10
1
0.1
0.01
Cs Rb Th U Ba Nb Ta La Ce Pb Sr Pr Nd Zr Hf Sm Eu Gd Tb Ti Dy Ho Y Er Tm Yb Lu Sc V
b)
trachyphonolite I
glass
Ap
sample/primitive mantle
10000
1000
100
10
1
0.1
0.01
Cs Rb Th U Ba Nb Ta La Ce Pb Sr Pr Nd Zr Hf Sm Eu Gd Tb Ti Dy Ho Y Er Tm Yb Lu Sc V

Fig.7

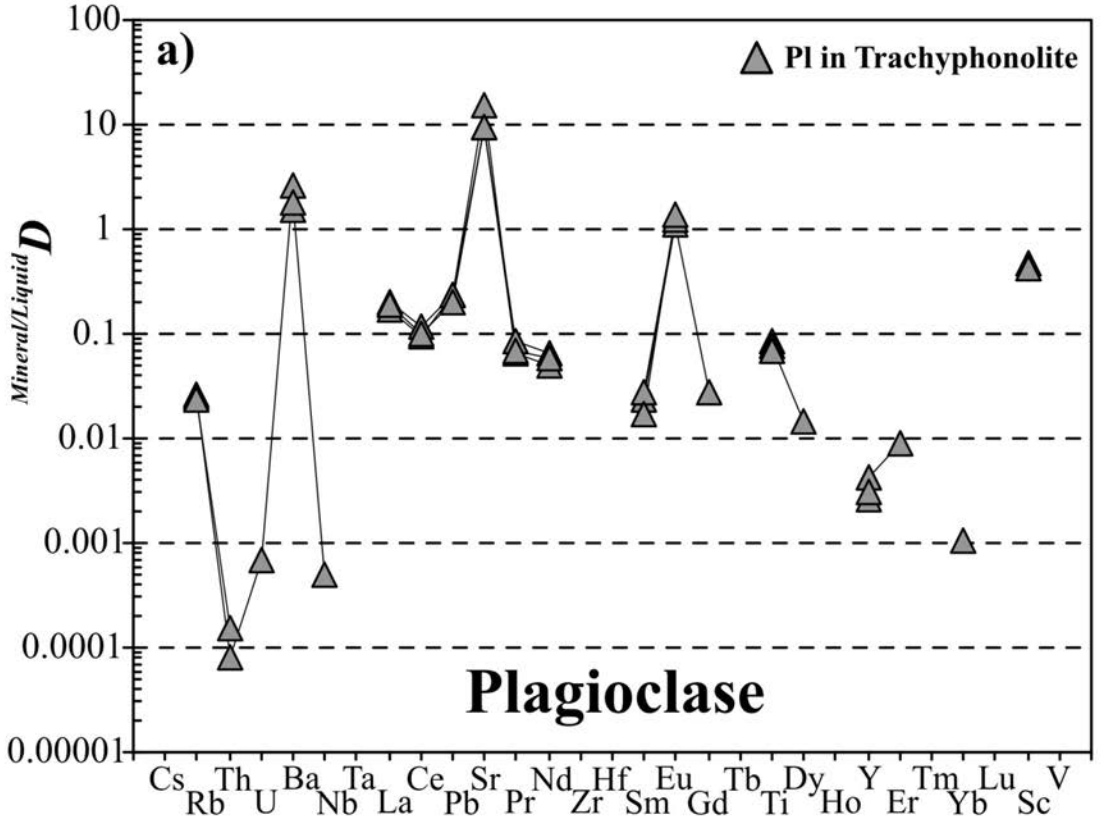
a)
Pl in Trachyphonolite
100
10
1
0.1
0.01
0.001
0.0001
0.00001
Mineral/Liquid D
Plagioclase
Cs Rb Th U Ba Nb Ta La Ce Pb Sr Pr Nd Zr Hf Sm Eu Gd Tb Ti Dy Ho Y Er Tm Yb Lu Sc V

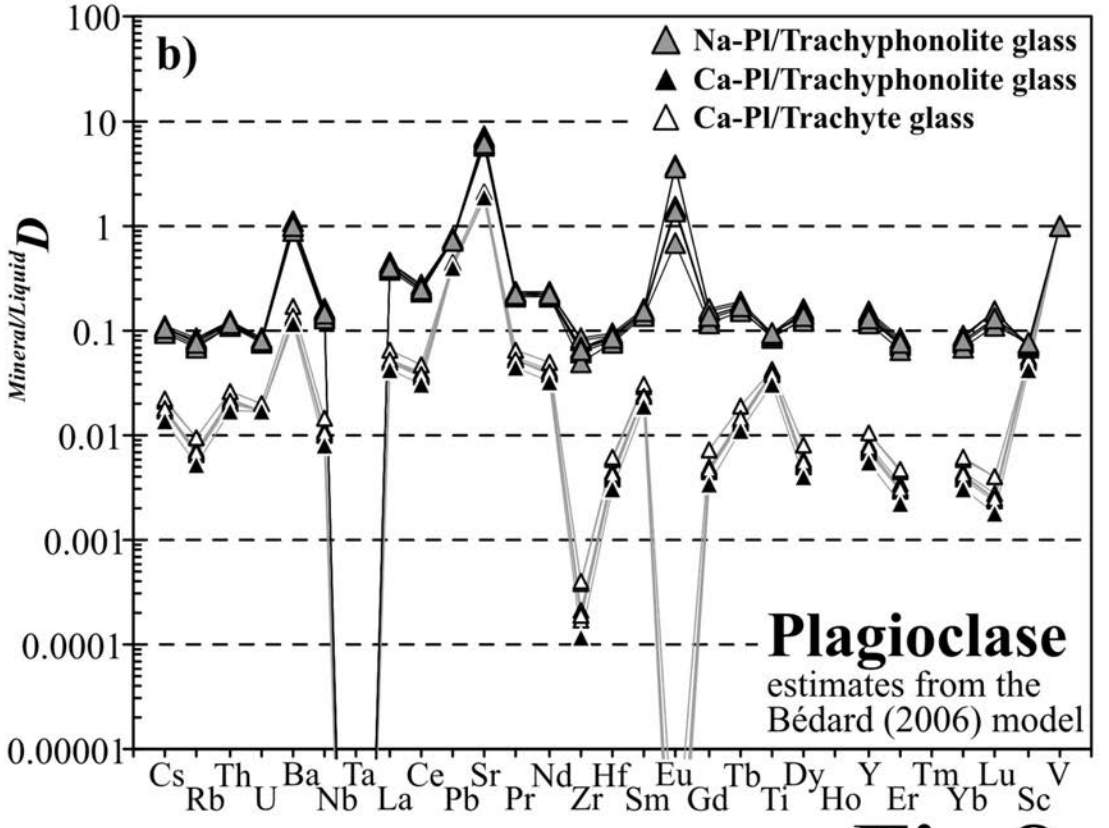
b)
Na-Pl/Trachyphonolite glass
Ca-Pl/Trachyphonolite glass
Ca-Pl/Trachyte glass
100
10
1
0.1
0.01
0.001
0.0001
0.00001
Mineral/Liquid D
Plagioclase
estimates from the
Bédard (2006) model
Cs Rb Th U Ba Nb Ta La Ce Pb Sr Pr Nd Zr Hf Sm Eu Gd Tb Ti Dy Ho Y Er Tm Yb Lu Sc V

Fig.8

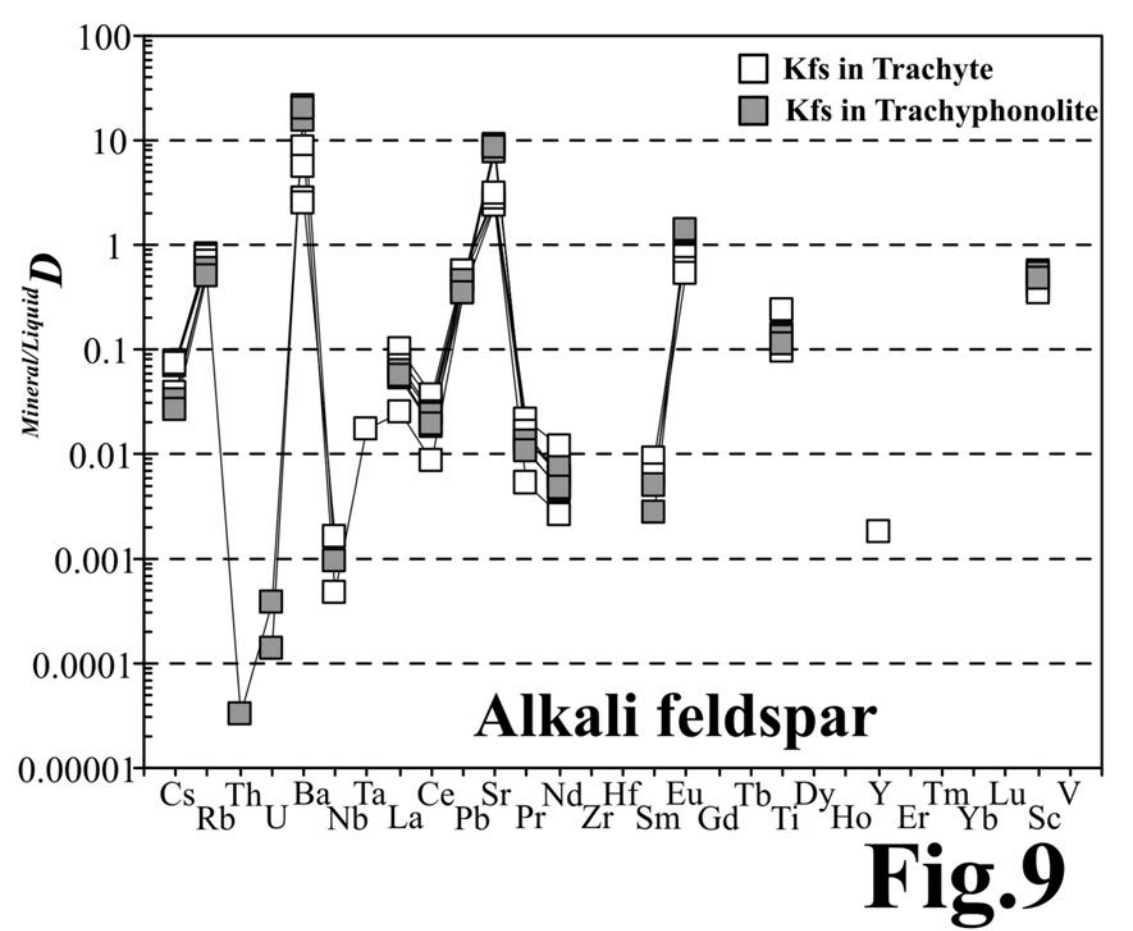
Kfs in Trachyte
Kfs in Trachyphonolite
Mineral/Liquid D
100
10
1
0.1
0.01
0.001
0.0001
0.00001
Alkali feldspar
Cs Rb Th U Ba Nb Ta La Ce Pb Sr Pr Nd Zr Hf Sm Eu Gd Tb Ti Dy Ho Y Er Tm Yb Lu Sc V

Fig.9

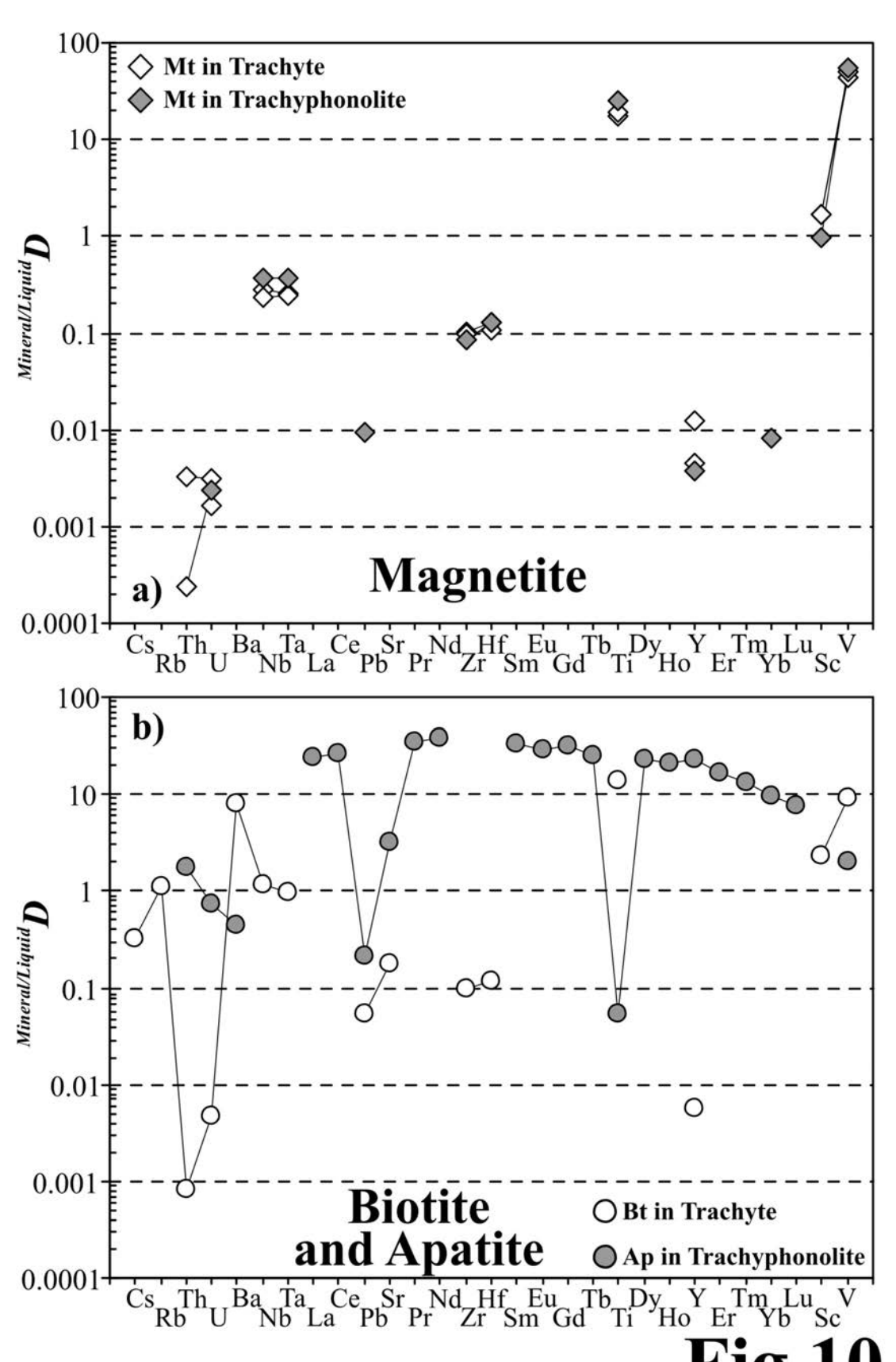
Mt in Trachyte
Mt in Trachyphonolite
Mineral/Liquid D
100
10
1
0.1
0.01
0.001
0.0001
a)
Magnetite
Cs Rb Th U Ba Nb Ta La Ce Pb Sr Pr Nd Zr Hf Sm Eu Gd Tb Ti Dy Ho Y Er Tm Yb Lu Sc V
b)
Biotite and Apatite
Bt in Trachyte
Ap in Trachyphonolite

Fig.10